Examining Roles of Residues of Plasmid TP228 Partitioning Proteins ParF and ParG in Interaction through Crosslinking of Mutant Cysteines

Brenton Setchfield

MSc by Research

University of York

Biology

February 2022

Abstract

Stable inheritance is vital for the survivability of plasmids, especially those that are low copy number. Low copy plasmids that utilise a partitioning system show greater genetic stability. Type I partitioning systems, also called ParABS systems, consist of three core components: ParA, the ATPase, ParB, the plasmid binding protein and *parS*, ParB's cis-binding site. The ParFGH system of the TP228 plasmid, found natively in *Salmonella enterica* serovar Newport, is one such system. It utilises a ParF meshwork that transports ParG bound plasmids to the midpoints of daughter cells during cell division. While the mechanism of the system is well understood, the interaction interface between the ParF and ParG proteins is not well characterised and presents a potential target for therapeutic treatment by preventing successful interaction of these two proteins in bacteria. This study focussed on mutations of the ParF and ParG proteins to replace residues of interest with cysteines. Constructed plasmids encoding these mutants were transformed into BL21(DE3) *Escherichia coli*. These proteins were overproduced and purified. A series of reactions were constructed containing combinations of either wild-type or mutated protein and cofactors before being treated with a BMOE crosslinking agent to elucidate on the physical interactions occurring between residues of interest in the reactions. These methods were successful in generating proteins but issues in stability and purity, particularly in ParF proteins, prevented visualisation of data on SDS-gels following crosslinking. Little to no appreciable conclusion regarding the interaction site of ParF and ParG was possible. This study did provide solutions to failings in the methods used to purify these proteins and presented some potential solutions to improve purification and storage of ParF. It was also possible to generate experimental improvements that would clarify data gained in similar studies on the interaction of this partitioning system.

Contents

List of Tables

List of Figures

Acknowledgements

I would like to thank Dr, Daniela Barillà and the Barillà research group for their support inside the lab and out. This project would not have been possible without their guidance and assistance. I would also like to thank all of my family and friends who supported me throughout this endeavour, be it in big ways or small.

Declaration

I declare that this thesis is a presentation of original work and I, Brenton Setchfield, am the sole author. This work has not been presented for an award at this, or any other, University or institution. All sources are acknowledged as references.

Chapter 1

Introduction

1.1 Role of Plasmids

There is no more fundamental factor when it comes to defining biological life than the stable inheritance of genetic material. Survival and evolution of millions of species over millions of years have depended upon selection and transmission of their genetic information (1). The densest and most biodiverse communities are lived in by bacteria, with a wide array of survival mechanics that can evolve and co-evolve alongside their neighbours, creating an ongoing drive in their evolution at much greater speeds than any other comparable living organism (2, 3, 4). Among the most notable genetic drivers of the accelerated evolution are plasmids. Plasmids' capacity to carry a wide array of survival genes and their ability to transfer horizontally between bacteria grant them several significant advantages over the more traditional vertical chromosomal transmission with regard to genetic heritability (5, 6). Genes harboured by plasmids are numerous but almost exclusively contribute to the plasmids' own stability. This is achieved through increasing their own transmissibility or by improving the survival of the host bacterium, especially in extreme environments or when competition is high. Common functions include transfer related proteins, toxic proteins such as peptides that affect competitors, degradative proteins that allow for additional sources of nutrition, virulence factors that make prokaryotes into pathogens and genes that encode for resistance factors to improve rates of host survival in inhospitable environments (7, 8, 9).

1.2 Issues of Plasmid Stability

Though plasmids are powerful evolutionary drivers, they are liable to competition and extinction as is any other form of genetic material. In order to prevent this, they can utilise multiple strategies. Some plasmids are able to take advantage of the stability of the bacterial chromosome by integration, reducing their risk of being lost at the cost of transmissibly, some take the opposite route, using transfer genes to spread their genetic material as far as possible, increasing the odds of a number of the plasmids surviving (6). This study focuses on plasmid stability systems that ensure the maintenance of plasmids from one generation to the next, when the cells divide. Unlike chromosomes, plasmids have no guarantee of surviving into both daughter cells when a cell undergoes cell division. High copy number plasmids propagate through a high number of replicates of the plasmid to allow for higher chances of the plasmid being inherited by both daughter cells, primarily by chance through free diffusion, though there is a minority of high copy plasmids that also focus a small number of the plasmid replicates to foci in the cell, increasing the chances slightly beyond random chance (10, 11, 12).

High copy number plasmids also suffer when a metabolic strain is present such as competition or the immune response of a potential host organism, which can lead to the cell

being overwhelmed (10, 13). Mathematically, plasmids would require a minimum of six copies for a 95% chance of passing a plasmid to both daughter cells through diffusion alone. Though as they are formed in the same position, more plasmids may be required, which can be an issue in a restrictive environment, particularly if said plasmids are large and would overwhelm the cell without inhibition of excessive DNA replication (12, 13). The issue of maintaining an equilibrium of freely diffusible plasmids for vertical propagation and reducing the metabolic stresses from plasmid replication in an environment that may not be conducive to the host cell's survival has led to the increase in developed strategies for improving the odds of inheritance in both daughter cells while reducing the resulting metabolic strain. These mechanisms are referred to as plasmid stability systems (14).

1.3 Stability Systems

There exist multiple mechanisms that stability systems undertake. Some use a combination of producing a long-lived intracellular cytotoxin alongside a corresponding short-lived antitoxin that are both encoded on the plasmid. With such a system, any daughter cell that does not inherit the plasmid is killed by the cytotoxin still present in the cytoplasm when the antitoxin expires, resulting in lethality if the plasmid is not passed on. Systems like this are called post-segregational killing systems, addiction modules or simply toxin-antitoxin systems. One example being the Phd-Doc system of phage plasmid P1 found in *Vibrio cholerae*, which encodes the Doc toxin that targets the ribosome and inhibits translation alongside the Phd protein that prevents inhibition of the ribosome (15, 16, 17, 18). Though this method does not guarantee a greater vertical inheritance of the plasmid, it does ensure that the P1 host cannot be outcompeted by a plasmid free *V. cholerae*.

Another example of such a stability mechanism is the Cre-*lox* system, expressed in recA *E. coli*. This system decreases the metabolic strain of plasmid production by separating interlocked plasmids that would otherwise be impossible to disseminate to separate daughter cells. This is performed by using its Cre protein to bind to a pair of *lox* sites on interlocked plasmids that have become entangled and recombine them into a dimer. This dimer is then separated back out into two unlinked and therefore independently heritable plasmids, thus reducing the metabolic cost of producing additional heritable plasmids to prevent the possibility of multicopy plasmid instability. (16, 18)

A more common form of plasmid stability strategy involves partitioning systems. These systems have evolved a mechanism to physically move copies of the plasmid to opposite ends of a cell, such that they are effectively guaranteed to pass a copy of the plasmid to both daughter cells, which is especially effective in low-copy number plasmids and plasmids whose stability is dependent on selective pressure from external sources (18, 19). These

systems are best characterised in Gram negative bacteria such as *E. coli* and *Salmonella* Newport. They are broadly comprised of three components: an ATPase protein: ParA, a centromere-binding protein that binds the *cis*-acting plasmid partition site: ParB and the cisregulatory region located either upstream or downstream of the partitioning operon: *parS* (14). The ParA forms either dimers or higher-order oligomeric structures within the cell that are responsible for the movement of the ParB-plasmid complex (20, 21). ParB triggers the ATPase activity of ParA, which results in the physical movement of the ParB-plasmid complex along the ParA structure, causing disassembly of the ParA as it moves and delivering the plasmid to the cell pole or, in some cases, a specific intracellular location (21, 22). There are three broad categories of partitioning systems, each based around the type of ParA protein the system utilises.

1.4 Partitioning Systems

1.4.1 Type III Systems

Type III partitioning systems are typified by a tubulin-like ParA analogue, a great example of which is the TubZ of the TubZRC partitioning system, initially identified in the PXO1 plasmid of *Bacillus anthracis* and later the C-ST prophage of *Clostridium botulinum* (23, 24). This system does possess an additional protein that does not conform to the ParABS cassette template, TubY, which serves a dual role in activation of the TubZR*C* operon and disassembling of the TubZR*C* complex (25).

1.4.2 Type II Systems

Type II partitioning systems are present in a wide range of prokaryotes. Type II ParA analogues possess a great variation in secondary structure across different systems, but a well conserved actin-like tertiary structure that forms filaments that resemble eukaryotic actin structures. Unlike eukaryotic actin, type II actin segregation proteins are apolar and elongate at both ends, resulting in a pushing system, rather than cytoskeletal pulling (26). An example of such a system is the ParMR*C* partitioning system found in the R1 antibiotic resistance plasmid in *E. coli* (27).

1.4.3 Type I Systems

Type I partitioning systems were the first to be identified and are characterised by the presence of a Walker box region with a general motif G54xGK(T/S) in their ParA protein.

They are the most common type of partitioning system encoded by plasmids by a wide margin, even so far as to be further divided into subtypes Ia and Ib based on the layout of the operon that encodes the proteins (21, 28). The ParAB*S* system, which was initially

discovered in the P1 plasmid, exemplifies the type Ia system, where the *cis*-binding partitioning site of the plasmid is downstream of the operon that encodes the ParA and ParB proteins (29). A type Ib partitioning system has its *cis*-acting site immediately adjacent to the operon that encodes the ParA and ParB homologues, much like the type II and III systems. Moreover, a general trend indicates that ParA and ParB proteins are smaller in type Ib systems than in type Ia systems (21). In the case of the ParFG*H* system, which this study focusses on, the *parH cis*acting site partially overlaps the promoter. This has a secondary effect of steric occlusion of RNAP by ParG binding to the *parH* site (30) (Figure 1).
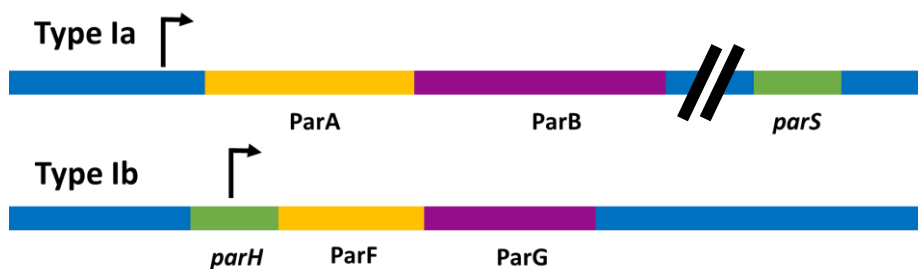
Figure 1: Type 1a and 1b Partitioning System Cassettes

Cartoon showing the type 1a system, ParAB*S*, which shows longer coding sequences and a downstream cis-acting site, and the type 1b system, ParFG*H*, which shows shorter coding sequences and a cis-acting site that partially overlaps with the -10 box

1.5 The ParFG*H* System

1.5.1 Overview

This study focuses on the ParFG*H* partitioning system, a type Ib system found in the TP228 plasmid. This system is found natively in *Salmonella* Newport and its segregation is most commonly studied in *E. coli*. The TP228 plasmid is a large, low-copy number plasmid that encodes resistance to multiple antibiotics, including tetracycline, spectinomycin and various sulphonamides. Resistance to such a variety of antibiotics can prove an issue, though outbreaks of *Salmonella* Newport specifically are a rare occurrence, with only 167 reported hospitalisations due to *Salmonella* Newport infections specifically in the US between July and September of 2020. Infections from various *Salmonella* and *E. coli* species that can also be conjugatively transferred with the TP228 plasmid are much more common. (31, 32).

The ParFG*H* system of TP228 is an example of a ParAB*S* system. It encodes a ParA homologue, called ParF, and a ParB analogue, called ParG, which binds with the *parS* analogue, *parH. parH* is a *cis*-regulatory site which is found immediately upstream of the ParG and ParF open reading frames, overlapping the promoter (30, 33). The contributions of

specific residues involved in the formation of the ParFG complex are currently not well characterised, especially given the non-structured N-terminus of the ParG.

1.5.2 ParF

ParF is a 22 kDa homologue of ParA that contains a deviant Walker A box, consisting of PKGGSGKTT from residues 9-17 rather than the canonical GxxxGK(T/S) for ATP-binding ParA-like protein. (28, 34). The structure of ParF displays a strong structural similarity to fellow partitioning system protein Soj of *Thermus thermophilus* and *E. coli* membrane associated ATPase MinD, which plays a role in topological determination of the cell poles prior to division (35). This is emblematic of the wide range of functions that both Walker box and ParA-like proteins perform, with MinD a membrane protein and ParF and Soj found in the cytoplasm also demonstrating differences in location of activity (28). The ParF secondary structure consists of seven β-sheets surrounded by eight α-helices, starting with the N-terminal β1 sheet and alternating between β-sheets and α-helices until the adjacent α7 and α8 helices at the C-terminus, with the deviant Walker A box in the β1 sheet and the Mg^{2+} ion binding Walker B box across the C-terminal end of the α3 helix and into the N-terminal end of the β4 sheet (34). The Mg^{2+} ions bound to the Walker B box are able to act in conjunction with the Walker A box to position a triphosphate nucleotide, natively ATP but AMP-PCP for the purposes of imaging a non-hydrolysable conformation, which enables the ParF to dimerise when bound to a triphosphate nucleotide (34, 36) (Figure 2, 3). The binding to the nucleotide is established by the K15 residue of deviant Walker A box contacting the β phosphate of the nucleotide, the Mg^{2+} ion recruited by the Walker B box along with the D37 and D38 residues of the β2 sheet (34). The D82 of the β4 sheet cooperate to stabilise the positioning of the phosphates. The D111, F112, G116 and V121 residues of the α5 helix are implicated in maintaining the ribose sugar in a 3' endo pucker configuration, stabilising the nucleotide (36, 37). There is also a proline residue at position at 104 in a proline rich region of the β5 sheet that causes hyperactive ATP hydrolysis when mutated to alanine by altering the shape of the catalytic pocket, contrary to the very low levels of ATPase activity normally observed in WT ParF. Similar reactions occur in the R169 residue of the α7 helix and the G179 residue which is well conserved after the α7 helix across ParA homologues (37). Both of these residues contact the triphosphate nucleotide bound by ParF (37, Figure 3).
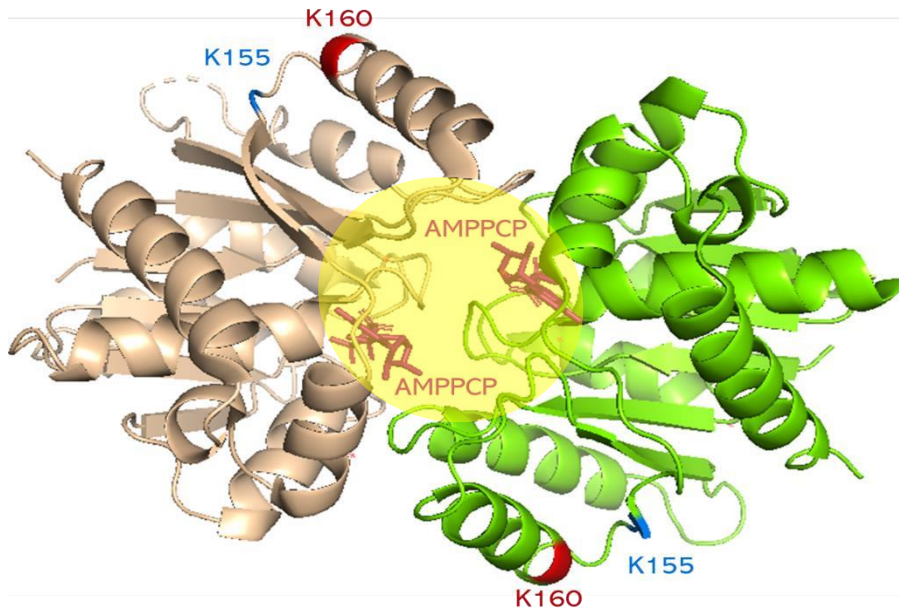
Figure 2: WT ParF Homodimer in ATP-bound configuration

Model showing the structure of a ParF homodimer with associated cofactors. Colours show different monomers. ATP analogues and lysine residues at positions 155 and 160 are labelled. The ATP/ParG binding pocket is highlighted yellow (66)

The *in vivo* cellular mechanism and function of ParF depends on its aforementioned capacity for dimerisation nucleotide due to a conformational change caused by binding to a triphosphate. The homodimerisation occurs at the site of nucleotide binding, which further stabilises the bound nucleotides' 3' pucker conformation. Key residues that mediate the interaction of two ParF-ATP monomers are the K64, V89, M96 residues, with M96 specifically connecting to the binding monomer partner's M96 residue (34). Upon forming stable homodimers, ParF becomes capable of forming dimer-of-dimer homomeric tetramers. These tetramers each have two pairs of interaction sites on opposite sides of the tetramer, known simply as interaction site 1 (I1) and interaction site 2 (I2). By binding of an I1 to an I2, the proteins can form an octamer while leaving one of each type of interaction site free at either end of the structure. With continued attachment of additional tetramers in this repeating tessellation pattern of tetramers, a stable filament can form. This structure is broadly found as a lattice associated with the nucleoid in the cell and, unlike other ParA proteins, can bind nonspecific DNA (38, 39).
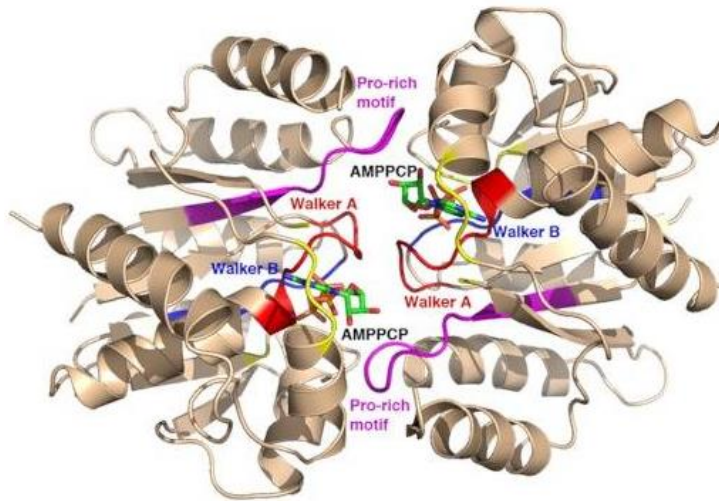
Figure 3: ParF Sites of Functional Importance

Model showing the structure of a ParF homodimer with associated AMPPCP. Colours show different functional sites.

(Figure from Schumacher MA, Ye Q, Barge MT, Zampini M, Barillà D, Hayes F. (2012). Structural Mechanism of ATP-induced Polymerization of the Partition Factor ParF. Journal of Biological Chemistry. 287(31): 26146-26154

1.5.3 ParG and parH

The site-specific DNA-binding protein of the ParFG*H* system is the ParG protein. It is an 8.6 kDa protein. It consists of a C-terminal ribbon-helix-helix domain and an N-terminal unstructured domain (Figure 4). ParG has a similar structure to the MetJ DNA binding protein found in *E. coli* that is responsible for repression of methionine synthesis and regulation of transcription as well as the Arc repressor that acts as the switch between lysis and lysogeny of the P22 bacteriophage that impacts *Salmonella* species (40, 41). The C-terminal helix-helix region allows for homodimerisation and the β-ribbon regions allow for the binding of the ParG homodimer to the *parH* site. The binding of the ParG homodimers to the *parH* site also acts as an autoregulator by steric occlusion to the operon's -10 box, preventing expression of additional ParF and ParG mRNA in similar fashion to the aforementioned MetJ and Arc proteins. This cements the reason for the system to be type Ib rather than Ia; the proteins are small enough and the *cis*-site can be used as an autoregulator without need for additional production of a third protein (30, 40, 41). The binding of ParG to *parH* results in recruitment of more ParG homodimers that bind along the *parH* region to repeating half-sites of 16 base pairs, they are able to bind in tetramers and even octamers when concentration increases. This binding is also partially dependant on the unstructured N-terminus; ParG truncations of Δ9, Δ19 and Δ30 all demonstrated the ability to homodimerise with each other and wild-type ParG as if untruncated but were not able to form tetramers or octamers, demonstrating the N-termini's role in oligomerisation. (30, 34) The Δ19 and Δ30 also demonstrated a failure to repress the expression of the genes. Though the Δ30 truncation does cause loss of several residues from the β ribbon, which is known to partake in *parH* site binding, the Δ19 does not, implying a role for the N-terminus in DNA binding. This DNA binding is theorised to be due to positively charged residues such at the K5, H7, K11 and K12 forming transient interactions with the negatively charged

backbone of the DNA to bring the β ribbons close enough to bind the specific site (30, 34, 42).

Binding of multiple dimers to the *cis*-regulatory partition site *parH* causes a shape change in the N-terminal tail of the ParG dimers, causing the tail to assume a more structured conformation. This region contains the R19 residue that acts as an arginine finger and increases the ATP hydrolytic activity of nearby ParF oligomers by inserting into the ATP binding pocket of the ParF dimer, resulting in the disassembly of the ParF higher order structure and transport of the ParG-plasmid complex (34, 43). The disassembly of the ParF structure following interaction with a ParG-plasmid complex prevents any additional ParG-plasmid complexes from moving in the same direction until a new ParF structure has reassembled (36, 34, 46). This allows for more effective separation of plasmids, moving them to opposite ends of the chromosome.

1.5.4 The Venus Flytrap Mechanism

The transport mechanisms by which the three different partitioning systems move the plasmid differ. For the ParFG*H* system, a Venus Flytrap model has been proposed. The mechanism involves a ParF meshwork that coats the nucleoid. The ParG-plasmid complex is captured by this meshwork, causing it to oscillate across the nucleoid. This requires the
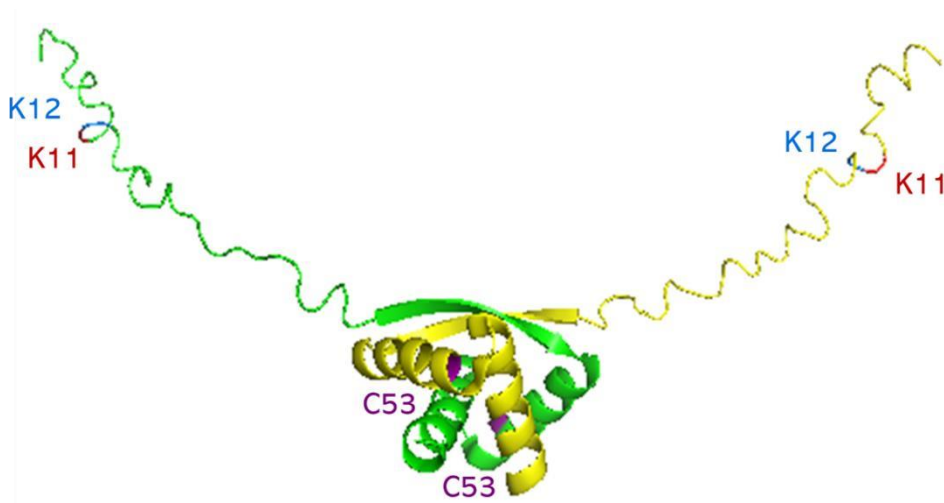
Figure 4: WT ParG Homodimer

Model showing the structure of a ParG homodimer. Colours show different monomers. Lysine residues at positions 11 and 12 and Cysteine residue at position 53 (66)

entire system to be present as without ParG or *parH*, a single static ParF meshwork is observed (36). The ParF matrix is thought to capture any plasmid after DNA replication, this capture of the loose plasmid is where the model derives its name, the ParF matrix representing the Venus Flytrap and the ParG-bound plasmid the captured fly. This model has the additional implication that the partitioning does not occur by moving plasmids to the extreme cell poles, as is the case in type II and type III systems (44, 45). The placement of these plasmids is determined by the separation of two plasmids on the ParF meshwork. One

plasmid is found in the ParF dense advancing region and one is found in the less ParF-dense lagging tail. During cell division, the two daughter cells express actin-like polymer bundles in the daughter cells that are used to capture genetic material, usually chromosomes (36, 46). These bundles will capture the plasmid following separation from the lagging strand, which is dissembled by the ParG induced ATP hydrolytic activity of the ParF monomers. The ParF meshwork will then carry the other plasmid in the other direction. Further oscillation of the meshwork across the nucleoid will continuously reset the plasmids at midpoints of the daughter cells' nucleoid until cell division occurs (36). This ensures any ParG-plasmid complexes end up separated on the nucleoid. A mechanism like this allows the immediate capture and separation of a small number of plasmids within the cell, maintaining their positions away from each other, increasing the likelihood of being at opposite ends of the dividing cell. Is also likely that the plasmids are attached to different daughter chromosomes following separation, thereby partitioning the plasmids to different daughter cells with low-copy number by tracking daughter chromosomes. The movements of multiple plasmids in the meshwork would eventually cause one to become left by a lagging tail, preventing them being caught by the same daughter cell. In the Venus Flytrap model, the ParF meshwork penetrates the entire nucleoid region and allows ParG plasmid complexes greater movement than would occur with a model only utilising movement of the plasmid on the surface of the nucleoid. It also overcomes the transient and unreliable dependence on diffusion gradients that would occur in a diffusion-ratchet model by providing a structure to associate with, the ParF lattice (36, 46, 47, 49, 50, 51) (Figure 5).
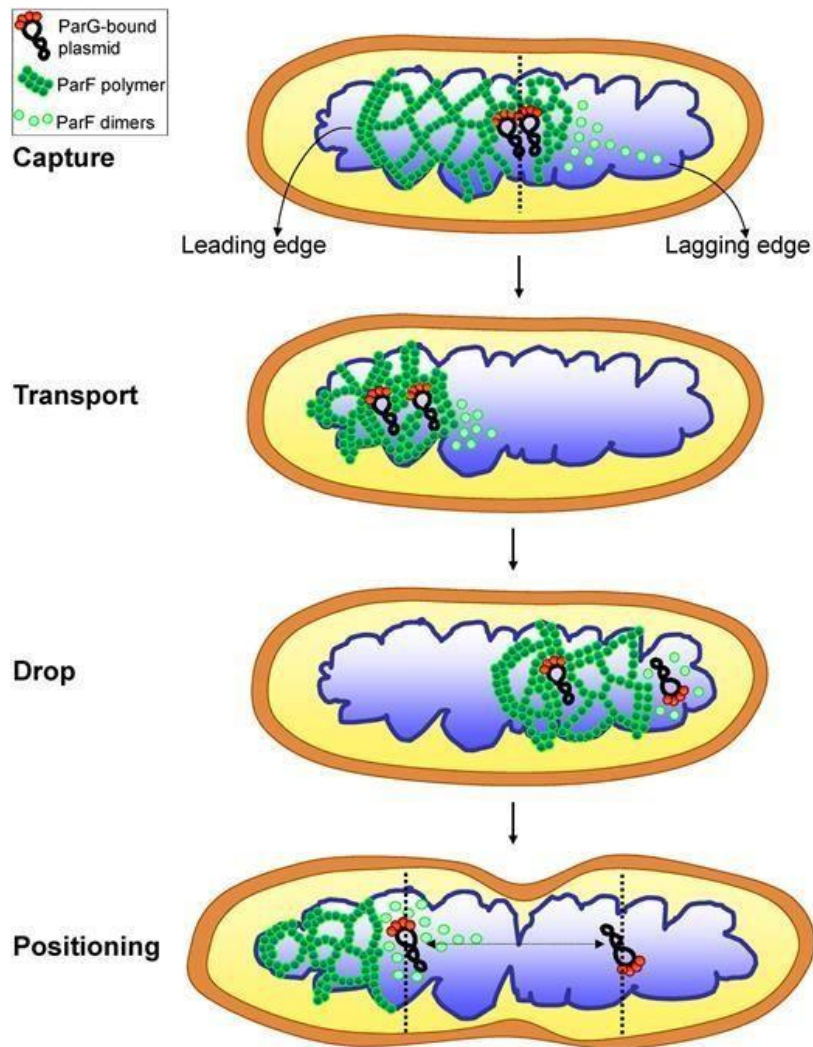
Figure 5: The Venus Flytrap mechanism

Cartoon showing a pair of ParG bound plasmids being engulfed by the ParF mesh and moved to the opposite daughter cell midpoints until one is detached from the lagging edge of the mesh by intersecting polymer bundles.

(Figure from Caccamo M, Dobruk-Serkowska A, Rodríguez-Castañeda F, Pennica C, Barillà D, Hayes F. (2020) Genome Segregation by the Venus Flytrap Mechanism: Probing the Interaction Between the ParF ATPase and the ParG Centromere Binding Protein. Frontiers in Molecular Biosciences. 7(108)

1.5.5 Project Aim

This project aims to probe the interface of the interaction between ParG and ParF; ideally to identify the roles of specific residues in the interaction pocket. Each residue under examination that was identified for analysis in this study was converted to cysteine. This allows β-mercaptoethanol to reduce the sulphur atoms in the cysteines, covalently bonding the proteins at these residues. ParG mutants were incubated with ParF mutants to allow crosslinking to form heterodimers if the two residues were close enough to be interacting. This would reveal which residues could contribute to the interface of the two proteins and provide insights into the role of the wildtype residues in the interaction.

Ideally, once the active site is located and established, future studies could develop a method of preventing wild-type interactions between the proteins. This method could be via a competitive inhibitor that would bind to either protein, rendering them sterically incompatible, or a non-competitive inhibitor to that could affect the tertiary structure of these proteins to prevent interaction. This could be achieved through steric occlusion of the ParF

and ParG active sites or through non-competitive inhibition that alters either protein's tertiary structure, separating vital interacting residues. It could also be via a protein that mimics ParG's activity without binding *parH*, dramatically increasing ParF's ATPase activity and preventing formation of a stable meshwork. Such an agent could be used as the active ingredient in a novel antibiotic that would disable the partitioning system of the bacteria carrying them, thus disrupting the stable inheritance of plasmids that commonly carry antibiotic resistance genes. (7, 8, 9) This would result in antibiotics with established resistances regaining efficacy in treating a proportion of the population of a pathogen with an inactive ParFGH system.

Chapter 2

Materials and Methods

2.1 Materials and Equipment

2.1.1 Biological Components

Plasmids

The plasmid used in this study was pET22b. It was chosen as a bacterial expression vector due to its ability to express high levels of inserted recombinant protein. As a practical matter for this study, it also conferred ampicillin resistance, allowing for selection of any cells that are successfully transformed with the plasmid. The expression of inserts is under the regulation of a T7 promoter and controlled by a *lacI* operator, allowing for theoretically high concentrations of recombinant protein production that would be inducible by addition of IPTG to a culture of the cells (52, 53). Plasmids encoding for one of ParF or ParG, with the addition of a series of C-terminal histidine residues used to form a His-tag, were supplied by the Barilla group to be used in plasmid purification.

Strains

Table 1: Cell Strains and Genotypes

Cell Strains	Genotype
DH5α	F–Φ80lacZΔM15 Δ(lacZYA-argF) U169 recA1 endA1 hsdR17 (rK–, mK+) phoA supE44 λ– thi-1 gyrA96 relA1
BL21(DE3)	fhuA2 [lon] ompT gal (λ DE3) [dcm] ΔhsdS
XL10	TetrD(mcrA)183 D(mcrCB-hsdSMR-mrr)173 endA1 supE44 thi-1 recA1 gyrA96 relA1 lac Hte [F´ proAB lacIqZDM15 Tn10 (Tetr) Amy Camr]

Table showing all cell strains and associated genotypes that were used for production of desired plasmids or proteins in this study. DH5α and BL21(DE3) used in plasmid production and XL10 used for protein production

XL10 Gold Ultracompetent Cells, hereafter referred to as XL10 Gold cells, were used for initial uptake of small amounts of plasmid, following PCR mutagenesis. The mutant plasmids were transformed into XL10 Gold cells which were grown and the plasmids harvested to give a high enough concentration to reliably transform DH5α cells.

DH5α cells were used in this study to generate plasmids at greater yields following production by XL10 Gold cells. DH5α cells were ideally suited for high plasmid yield on account of their *rec*A1 stability gene that reduces recombination, resulting in greater stability of target plasmids and *end*A1 that increases quality of dsDNA derived via miniprep, thus improving plasmid quality in this study (54).

BL21 (DE3) cells, hereafter referred to as BL21, were used for overproduction of the proteins. BL21 are well adapted for this purpose due to fewer proteases that could damage recombinant proteins. They are also adapted through introduction of the lacUV5 promotor to render T7 RNA polymerase inducible by IPTG, increasing expression of recombinant proteins. This system is added onto phage genome DE3, hence BL21 (DE3). These adaptations allow for inducible control with high expression, making this the ideal strain for recombinant protein expression (42, 55).

2.1.2 Media and Solutions

LB Broth: 5 g LB Miller Broth powder was dissolved in 200 mL ultrapure water by mixing. The solution was then sealed and sterilised by autoclave.

LB Agar: 11.1 g of LB Miller Agar powder was dissolved in 300 mL ultrapure water by mixing. The solution was then sealed and sterilised by autoclave.

RF Competence Solution 1 (RF1): 15% Glycerol; 50 mM Manganese Chloride; 30 mM Potassium Acetate; 10 mM Calcium Chloride; 100 mM Rubidium Chloride

Solution made to volume with MQ water, balanced to pH 5.8 and filter sterilised.

RF Competence Solution 2 (RF2): 15% Glycerol; 50 mM Manganese Chloride; 75 mM Calcium Chloride; 10 mM MOPS

Solution made to volume with MQ water, balanced to pH 6.8 and filter sterilised.

ParF Binding Buffer: 50 mM pH 8 Tris-HCl, 500 mM NaCl, 15 mM Imidazole, 10% Glycerol

ParF Wash Buffer: 50 mM Tris-HCl pH 8, 1 M NaCl, 85 mM Imidazole, 10% Glycerol

ParF Elution Buffer: 50 mM Tris-HCl pH 8, 150 mM NaCl, 300 mM Imidazole, 10% Glycerol

ParF Storage Buffer: 30 mM Tris-HCl pH 8, 100 mM KCl, 10% Glycerol

ParG Binding Buffer: 20 mM Tris-HCl pH 8, 500 mM NaCl, 15 mM Imidazole, 10% Glycerol

ParG Wash Buffer: 20 mM Tris-HCl pH 8, 1 M NaCl, 90 mM Imidazole, 10% Glycerol

Later ParG Binding Buffers contained no imidazole and ParG Wash Buffers were made with 25, 50 and 95 mM concentrations of imidazole if purification with the initial method was unsuccessful, as detailed in the purification protocol.

ParG Elution Buffer: 20 mM Tris-HCl pH 8, 500 mM NaCl, 400 mM Imidazole, 10% Glycerol

ParG Storage Buffer: 50 mM HEPES pH 8, 50 mM KCl, 10% Glycerol

Early storage buffers for both ParF and ParG contained DTT, which was later removed as it would interfere with the protein crosslinking assay.

15% SDS-gel Production (2 Gels)

Resolving Gel: 3.4 mL ultrapure water, 3.8 mL 1.5 M Tris-HCl pH 8.8, 150 µL 10% SDS, 7.5 mL 30% Acrylamide, 150 µL 10% APS, 6 µL TEMED

Stacking Gel: 2.7 mL ultrapure water, 500 µL 1 M Tris-HCl pH 6.8, 40 µL 10% SDS, 670 µL 30% Acrylamide, 40 µL 10% APS, 4 µL TEMED

Gels were made by first mixing the resolving gel and quickly pipetting 5 mL of the liquid into the 1 mM gel mould and adding a few drops of 70% ethanol to the top to remove air bubbles. The sample was then left to set for 30 minutes and the ethanol layer was then removed with paper towels. Next, the stacking gel was made and quickly pipetted onto the set resolving gel to fill the mould. The comb was quickly added and the gel was left for another 30 minutes for the stacking gel to set.

4-15% SDS-gels

For later in the study, Bio-Rad's Mini-PROTEAN® TGX™ 10 50 µL well Precast Protein Gels were used to ensure greater reliability and spread of the proteins in images.

SDS Loading Buffer

2x SDS loading buffer is comprised from 100 mM pH 6.8 Tris, 200 mM DTT, 4% SDS by volume, 0.2% bromomethyl-blue by volume, 20% glycerol by volume and made up to volume by dH_2O.

SDS Running Buffer

10x SDS Running Buffer was made by dissolving 200 g of Glycine, 60.4 g SDS and 20 g of Tris in 2 L of dH_2O. This buffer was diluted in dH_2O to 1x for use in gels.

Coomassie Brilliant Blue Stain and Destain

Coomassie Brilliant Blue destain was made by 50% methanol by volume, 10% acetic acid by volume and made up to volume with dH_2O. Coomassie Brilliant Blue stain was made by adding 2.5 gL^{-1} Coomassie Brilliant Blue powder to Coomassie destain.

2.1.3 Materials and Equipment

Centrifuges: The centrifuges used were a Thermo Scientific SL 16R, an eppendorf Centrifuge 5418 R and an Eppendorf Minispin Plus

Sonicator: Sonication was performed using a Bendelin Sonoplus HD2070 sonicator.

Fluorometre: Fluorimetry was performed using a Thermo Fisher Invitrogen Qubit 3 Fluorometer

Dialysis Tubing: The dialysis tubing used was ThermoFisher Scientific Snakeskin™ Dialysis Tubing with 22 mM internal diameter and a 7 kilodalton molecular weight cut-off (MWCO)**.**

2.2 Methods

2.2.1 Transformation

Competent Cell Preparation

A 10 mL liquid culture of DH5α or BL21 (DE3) cells was grown at 37°C to an OD_{600} between 0.4 and 0.6. The culture was incubated on ice for 10 minutes then centrifuged at 2200 RCF for 10 minutes. The supernatant was discarded and the cell pellet resuspended in 20 mL RF1 solution and incubated on ice for 90 minutes. It was then centrifuged at 2200 RCF for 5 minutes. The supernatant was discarded and the pellet was resuspended in 5 mL RF2 solution and incubated on ice for 15 minutes. The resuspended cells were then aliquoted in 500 μL samples, flash-frozen in liquid nitrogen and stored at -80°C.

Mutant Plasmid Construction

The solution for PCR was made up using Agilent Technologies' QuikChange Lightning SiteDirected Mutagenesis Kit in accordance with the manufacturer's instructions. The oligos being used as primers were made up to 100 μg mL^{-1}. All preparation was performed on ice unless specified otherwise (56).

The mixture was placed in the PCR cycler and heated to 95°C for 2 minutes followed by eighteen cycles of 95°C for 20 seconds, 60°C for 10 seconds and 68°C for 3 minutes and a final hold of 68°C for 5 minutes. The samples were then held at 10°C until they could be stored at 4°C.

The genes and parH sites were generated prior to the study by using a Phusion polymerase and a PFH-547 plasmid containing the entire ParFGH cassette, which was Sanger sequenced externally, with the results being interpreted manually.

Plasmid transformations into XL10 Gold Ultracompetent Cells

All plasmids used in transformation were purified to high concentration and sequenced externally; transformation only occurred if there were no mutations present besides the

desired residue (or no mutation in the case of the WT proteins) and the addition of the C-terminal His-tag used in purification.

To perform the transformation, 2 µL (10 Units µL^{-1}) of DpnI enzyme were added to the PCR reaction mixture and heated in a 37°C water bath for 5 minutes to degrade unmethylated DNA. An aliquot of XL10 Gold cells was thawed on ice and 45 µL of these thawed cells were mixed with 2 µL 1% β-mercaptoethanol and 2 µL of the DpnI treated DNA at 4°C to give one transformation mixture. Each mixture was then incubated at 30°C in a water bath for 30 minutes then heat shocked at 42°C for 30 seconds to trigger uptake of the plasmid into the XL10 Gold cells. The mixture was then incubated on ice for 2 minutes and then pipette mixed with 500 µL of NZY$^+$ that had been pre-heated to 42°C to aid in the cultivation of the cells. Following this, the solution was incubated at 37°C for 1 hour. 100 µL of solution was then plated onto a 100 µg mL^{-1} ampicillin agar plate. The remainder was centrifuged at 9300 RCF for 2 minutes, 100 µL of the supernatant was collected and the rest discarded and the pellet was resuspended in the collected 100 µL and the resulting culture was spread on a second plate. The plates were incubated at 37°C overnight.

Plasmid culture growth and plasmid extraction from transformant XL10 Gold Ultracompetent Cells and transformation into DH5α Cells

Purification of plasmids was performed using Qiagen QIAprep spin Miniprep Kits.

Following transformation on an agar plate, one colony was used to inoculate 20 mL of LB containing 100 µg mL^{-1} ampicillin. These cultures were grown at 37°C with agitation at 180 rpm overnight.

If overnight growth was successful, the culture was split into two 10 mL cultures and spun at 5600 RCF for 5 minutes. The supernatant was discarded and pellets were resuspended in 500 µL of chilled A1 buffer each and then split into two 250 µL samples each. Next, 250 µL of A2 buffer was added and the samples were inversion mixed and left at room temperature for 5 minutes to allow full cell lysis. Following this, 300 µL of N3 buffer was added and immediately invert mixed until the solution became colourless to ensure the precipitated DNA was alkalised and prepped for the binding conditions of the silica membrane in the miniprep column. These samples were then centrifuged at 5000 RCF for 7 minutes and 30 seconds to isolate the DNA. The supernatant was then collected and spun through the Qiagen Qiaprep filter tube for 5000 RCF for 3 minutes. 600 µL of AW buffer was then added to flush any additional cell debris into the elution fraction, which was then eluted. The DNA bound to the column was then resuspended by addition of 30 µL of AE buffer to the column and left for 1 minute to ensure the DNA was eluted from the binding membrane before centrifuging for 1 minute at 5000 RCF to collect the plasmid in the AE buffer. The DNA concentration was

measured using the Qubit Fluorometer and the remainder was labelled and stored at -20°C (57).

Plasmid Transformations into DH5α or BL21 Competent Cells

Transformations were performed by thawing a single aliquot of the relevant competent cells on ice, mixing 2 µL of pET22b plasmid (containing *parF*, *parG* or mutant variants) extracted from transformant XL10 Gold cells with 100 µL of competent DH5α or BL21 cells and storing this mixture on ice for 30 minutes. The sample was then heat-shocked at 42°C for 90 seconds and was then mixed with 400 µL of LB broth. The sample was then shaken at 180 rpm at 37°C for one hour to begin cell growth and then 100 µL of the resultant culture was spread onto an agar plate of 25 mL of Miller LB agar and left at 37°C to grow overnight. The agar on the plate contained 100 µg mL^{-1} ampicillin to select for cells that had taken up the plasmid.

2.2.2 Protein Production and Purification

Pilot Culture for Testing Induction and Solubility

10 mL of pre-warmed 37°C LB Broth was inoculated with a single colony of transformed BL21 cells. The culture was then grown at 37°C and shaken at 180 rpm until the OD$_{600}$ of the culture was between 0.6 and 0.8. At this point, 100 µL of the culture was taken and centrifuged at 5000 RCF for 3 minutes, the supernatant was discarded and the cell pellet was frozen at -20°C. The remaining culture was induced with IPTG to a final concentration of 1 mM. Another 100 µL sample was taken and similarly centrifuged at hourly intervals for the next three hours with all the pellets also stored at -20°C. This was to provide a demonstration of the induction of the protein production by IPTG over time.

To test for protein solubility, 2 mL of the remaining culture was taken and centrifuged at 5000 RCF for 3 minutes, the supernatant was discarded and the pellet stored at -20°C.

Large Scale Overproduction Culture for Protein Purification

20 mL of 37°C LB broth was inoculated with a single colony of successfully transformed BL21 and grown overnight at 37°C, shaken at 180 rpm. It was then poured into 300 mL of pre-warmed sterile LB broth containing 100 µg mL^{-1} ampicillin and grown at 37°C, shaken at 180 rpm until the OD$_{600}$ of the culture was between 0.6 and 0.8. Samples were taken and pelleted as in the pilot, followed by induction with IPTG up to 1 mM. The remainder was split into 50 mL tubes and spun at 8000 rpm for 15 minutes. The supernatant was discarded and the cell pellet was frozen at -20°C.

Protein Purification

150 mL liquid culture's worth of frozen pellets were resuspended in 10 mL of chilled Binding Buffer, lysozyme up to 7 μM and one crushed protease inhibitor tablet were added and mixed. The solution was then heated in a water bath at 30°C for 15 minutes. Then another 100 μL of lysozyme was added and the resuspended cell mixture was heated in the water bath at 30°C for a further 15 minutes. The mixture was then stored on ice and sonicated at 60% power for 15 seconds with 1 minute intervals for 12 cycles unless otherwise specified. It was then centrifuged at 7800 RCF for 30 minutes; the supernatant and pellet were individually collected as pre-flow soluble fraction and crude pellet, respectively. A sample of each was frozen for analysis in gels and the remainder was either discarded or used for protein purification.

Nickel Column Tandem Affinity Purification (TAP)

All purification was performed at 5°C. First, the column was loaded with 5 mL HIS-binding resin. Then 20 mL of water were passed through, followed by 25 mL of 1x Ni^{2+} solution and 20 mL of filtered Binding Buffer. Then the pre-flow soluble extract was circulated on the column and allowed to cycle for 90-120 minutes. Next, 30 mL of filtered Binding Buffer was passed through the column, collected and stored at 4°C. Then 50 mL of Wash Buffer was used to wash the column and was also collected and stored at 4°C. Next, 15 mL of Elution Buffer was passed through and collected in 1.5 mL fractions. Finally, 30 mL of stripping buffer was passed, followed by 30 mL MQ water and 30 mL 20% ethanol. The resin was then removed and stored in a solution of 20% ethanol at 4°C for future re-use.

Later in the process, following several unsuccessful purifications, an update to this process became necessary. When utilising the updated method to purify ParF, the Binding Buffer flowthrough was collected in three 10 mL fractions, the Wash Buffer volume was reduced to 30 mL and was also collected in three 10 mL fractions. The process was otherwise unchanged.

When purifying ParG, the Binding Buffer contained no imidazole and was collected in three 10 mL fractions, the Wash buffer was administered in three fractions of 6 mL and each was collected in four aliquots of 1.5 mL. The three Wash Buffer fractions contained imidazole at concentrations of 25, 50 and 95 mM, respectively. The process was otherwise unchanged.

Small Scale Batch Purification

First, 500 μL of HIS-binding resin was added to a 2 mL Eppendorf tube and spun at 9300 RCF for 1 minute and any excess ethanol was siphoned off with a pipette. The tube was

then filled with Milli Q water and shaken thoroughly before re-centrifuging and siphoning the water. 1x Ni^{2+} solution was added to the tube and shaken for 30 minutes at room temperature before being centrifuged and siphoned. The tube was then filled with filtered Binding Buffer and shaken thoroughly, centrifuged and was siphoned. The pre-flow soluble protein extract was then added and incubated for one hour at room temperature and then centrifuged and siphoned. The siphoned sample was collected for running on a gel. The resin was then washed with Binding Buffer, Wash Buffer and then Elution Buffer, shaken thoroughly, centrifuged and siphoned each time. The supernatant fractions were all collected. This method did not prove reliable for large scale purification due to the difficulty in separating the resin from the supernatant fractions.

Desalting Column Buffer Exchange

The desalting column was washed with 25 mL Milli Q water then 25 mL filtered Storage Buffer. Desalting was performed by passing 1.5 mL of the protein containing fraction through the column, then 2 mL of Storage Buffer, which was collected as it would contain the protein and finally washed out with 5 mL of filtered Storage Buffer. This was repeated for each sample to be determined and the 2 mL outputs were aliquoted into 200 µL aliquots and flash frozen in liquid nitrogen and stored at -80°C.

Dialysis Buffer Exchange

Following analysis of the purification fractions with Bradford assays and on SDS-gels, the most highly concentrated fractions were combined into samples of no more than 10 mL. These samples were then placed into dialysis tubing that was sealed at both ends. These samples were then added to 500 mL of Storage Buffer with no DTT and using Tris-HCl rather than HEPES in the case of ParG. They were stirred at 5°C, 300 rpm for between 6 hours and overnight then transferred into 500 mL of fresh Storage Buffer without DTT. If multiple tubes of the same protein were used, they were dialysed against 1 L of Storage Buffer together but remained in separate dialysis tubes. Following dialysis, each tube was split into 200 µL aliquots and a representative from each was analysed by Bradford assay. Any tube with a usable concentration of protein was flash frozen in liquid nitrogen and stored at -80°C.

Crosslinking Assay

Crosslinking solution was made to 50 mM Tris-HCl, 50 mM NaCl, 2 mM MgCl$_2$ and 0.25 mM Tris-2-carboxyethyl-phosphine (TCEP) which was made up to volume with dH$_2$O and balanced to a of pH 7.5 using concentrated potassium hydroxide. The required aliquots of ParF, ParG, ATP and the region of *parH* bound by ParF and ParG complexes to be used

were thawed on ice. The dimethyl sulfoxide was thawed at room temperature. The protein concentration in the crosslinking reactions in initial assays were made up to 10 µM to allow for adequate visibility of the proteins on SDS-gels. The ATP was added to 1 mM and was always accompanied by MgCl$_2$ up to 5 mM to allow the ATP to interact with the ParF proteins as it would in vivo (58). *parH* was added to 8 µM. The ParG, ParF, ATP and excised non-coding *parH* were all mixed with 19 µL of the chilled crosslinking solution in the combinations necessary to provide adequate controls and samples, as required by the assay. Following initial mixing, the reactions were stored at 25°C for five minutes. Then any reactions that were to contain bismaleimidoethane (BMOE) crosslinker were made up to 1 mM BMOE dissolved in dimethyl sulfoxide. The reaction mixtures were then pipette mixed and left at room temperature for 30 mins to allow the crosslinking to occur. The reaction was then stopped with 3.69 µL of 1% β-mercaptoethanol and run on an SDS Polyacrylamide gel as detailed in section 2.2.3.

2.2.3 Analysis Protocols

DNA Concentration Measurement

The plasmids and DNA used were from miniprep purifications.

Qubit HS reagent solution was made by diluting 1 µL of 200x HS reagent into 199 µL of HS buffer. Control standards were made from 190 µL of HS reagent solution and 10 µL of one of the two supplied standards. The test samples were made from 5 µL of a 1 in 10 dilution of the purified test DNA in Milli Q water with 195 µL of the HS reagent solution. The dsDNA high sensitivity setting on the fluorometer was used to allow the concentration of the original sample of purified DNA to be calculated.

SDS Polyacrylamide Gel Electrophoresis

Any stored cell pellets were resuspended in water to restore them to the volume they were at before the supernatant was removed. 20 µL of each sample was then mixed with 20 µL of a 1:9 mixture of 1% β -mercaptoethanol and SDS Loading Buffer Stain. These samples were then heated at 90°C for 10 minutes to denature any proteins present. The gels were submerged in SDS running buffer and loaded with 10 µL of Pierce Unstained Ladder and 20 µL of each sample into the wells in lab-made gels or 20 µL of Pierce Unstained Ladder and 40 µL of sample in the case of pre-cast gels. When Pierce Unstained Ladder was unavailable, Thermofisher PageRuler Prestained Protein Ladder was used with unchanged volumes. Lab-made gels were run at 150 V for 30 minutes and then at 190 V until the dye front had only just cleared the gel. Pre-cast gels were run at 200 V until the gel front cleared the gel.

The gel was then removed and incubated in Coomassie Brilliant Blue Stain at room temperature on a shaker for 1 hour, then the Coomassie Stain was removed and the gel was washed with tap water and submerged in destain solution and left on a shaker for at least five hours or until it was ready to be imaged. The gel was then washed in tap water and imaged in a Bio Rad gel doc.

Bradford Assay

Test samples were made up with 795 µL of Milli Q water, 200 µL chilled Bradford's Reagent and 5 µL of the sample to be measured. Standards were made with 200 µL chilled Bradford's Reagent, 0-12 µL of 2 µg mL^{-1} BGG in 2 µL intervals and made up to 1 mL with MQ water. All ODs were measured at 595nm. The standards were used to plot a concentration standard line to measure the test samples against. Standards were made fresh and re-measured for each group tested.

Chapter 3

Results and Discussion

3.1 Construction of Mutant Protein Encoding Plasmids

As the first step in generating mutant plasmids, pET22b plasmids, which contained the gene encoding for either ParG or ParF fused to a C-terminal His-tag were transformed into DH5α cells.

In order to create the mutant forms of the ParF and ParG proteins, residues to be targeted for mutagenesis had to be identified. From previous work performed in the Barillà group by Dr. Cecilia Pennica and from the results published by Zhang and Schumacher, the ParF-K155C and ParF-K160C mutants and the ParG-K11C and ParG-K12C mutants, as shown in figures 2 and 4, would be reliable test subjects for this study. This was because they had shown strong evidence of interaction during these studies, albeit using different methodologies (59). Investigations involving cross-linking followed by mass spectrometry had highlighted interactions between these residues in the ParF and ParG proteins and a partial ParF-ParG complex structure also supported these findings (59).

In order to produce the desired mutant proteins, the above plasmids were used, each containing the wild-type form of one of the two genes. Using an online tool, primers that would introduce the intended mutations into the gene were designed. Mutation construction relied on the QuikChange Lightning Site-Directed Mutagenesis Kit in conjunction with PCR to create a series of new plasmids. The wild-type plasmids were incubated with the mutagenic primers and subjected to PCR. The PCR products were then treated with Dpn1 to degrade the original copies of the plasmids due to their being methylated and the new mutant plasmids, not being methylated, should not have been affected. This would theoretically only leave mutant plasmids in the solution.

The plasmids were introduced into XL10 Gold Ultracompetent cells and the transformants grown on ampicillin plates. Initially, there was no successful growth from any cells when plated. This was attributed to either a failure in uptake of the plasmid or failure of the PCR process to produce mutated plasmids. The first issue was corrected using a 42°C heat block, rather than a 42°C water bath, to ensure a more efficient heat transfer over a shorter window during heat shock. These modifications resulted in colony formation in the case of all plasmids on plates of high and low ampicillin concentration, implying a successful uptake of a whole plasmid. The second issue was tackled through a repeat of the PCR with an increase in concentration of wild-type template plasmid in each PCR cycle to 50 ng to increase the amount of plasmid available for mutation and replication during PCR. The above adaptations were henceforth used as the primary method of mutant plasmid synthesis and resulted in usable plasmid containing cells. It is worth noting at this stage that the

plasmids were only confirmed to contain the ampicillin resistance gene and not necessarily containing correct forms of the intended mutants, which remained to be tested.

The plasmid containing XL10 Gold colonies were used to inoculate two liquid cultures of each mutant and grown at 37°C overnight in preparation for plasmid purification. Plasmids were purified from each liquid culture and DNA concentration was measured by Qubit quantitation. Both samples of *parG*-K11C plasmid culture extraction yielded no plasmid. The *parF*-K160C plasmids resulted in concentrations of 11.1 and 15.6 µg mL^{-1} and the *parF*-K155C plasmids resulted in greater concentrations of 20.2 and 23.8 µg mL^{-1}. Samples of the higher concentration samples were sent for DNA sequencing externally by Eurofins Scientific to ensure that the point mutations had occurred correctly in the plasmids and that no additional mutations had occurred in any of the genes' sequences. These analyses were not sufficient to draw any conclusions, most likely due to the concentration of plasmid sample being too low. The mutant plasmid synthesis of the *parG*-K11C plasmid was repeated without methodological change until XL10 Gold cells transformed with the results of said mutation grew successfully, at which point those plasmids were purified.

A sample of the extracted *parG*-K11C mutant plasmid and both wild-type containing plasmids were transformed into DH5α cells for further plasmid production. This was done to produce a plasmid sample of high enough concentration for accurate sequencing of the *parG*-K11C plasmid and to increase the number of wild-type plasmids to meet the requirement to sustain both expression of wild-type proteins and to use as template plasmids for any further mutant plasmid synthesis that would be necessary.

Following growth of the DH5α transformants, colonies containing the parG-K11C plasmid were grown in four liquid cultures and the plasmids were purified. These plasmids had concentrations of 33.7, 41.7, 38.1 and 39.7 µg mL-1. Two samples of the 41.7 µg mL-1 sample were sent for sequencing. Further amplification of the samples by were required to obtain readable plasmid sequences for all the mutant containing plasmids. This was achieved by PCR and plasmid purification to maximise both the number of desired plasmids and their relative purity within the samples.

The wild-type containing plasmids were transformed into the BL21 strain for overexpression. The wild-type parF and parG containing plasmid BL21 plates all presented colonies and a 10 mL pilot expression was performed, with the intention to test the production of the wild-type proteins for use as a control to compare the mutants to. The samples were run on a 15% SDS polyacrylamide gel to analyse the outcomes.

3.2 Induction and Purification of Proteins

3.2.1 WT ParF

The WT ParF pilot overproduction gel demonstrates a steady increase in intensity of the thin band around 25 kDa over the induction period. This band is expected to be the ParF protein on account of being the only one in the three induction lanes of Figure 6 to continue increasing in intensity for this period. With regards to the overall protein production during the induction period, Figure 7 demonstrates little to no significant increase in the global amount of protein produced outside the 25 kDa band, further cementing it as the ParF protein.

Figure 6 demonstrated successful induction of wild-type ParF, visualised as a band just under 25 kDa, which is consistent with the expected 22 kDa band. The presence of a significantly greater 25 kDa band in the soluble fraction over the insoluble fraction demonstrated that ParF is soluble. However, the lack of any visible protein on the insoluble fraction suggests that any insoluble proteins were not visualised on Figure 6. Although this may lead to some doubts over the proportion of soluble to insoluble ParF, Figure 6 definitively shows a significant presence of soluble ParF protein, implying that the soluble fraction of a large-scale overproduction would generate enough soluble ParF for crosslinking given adequate purification (Figure 6).
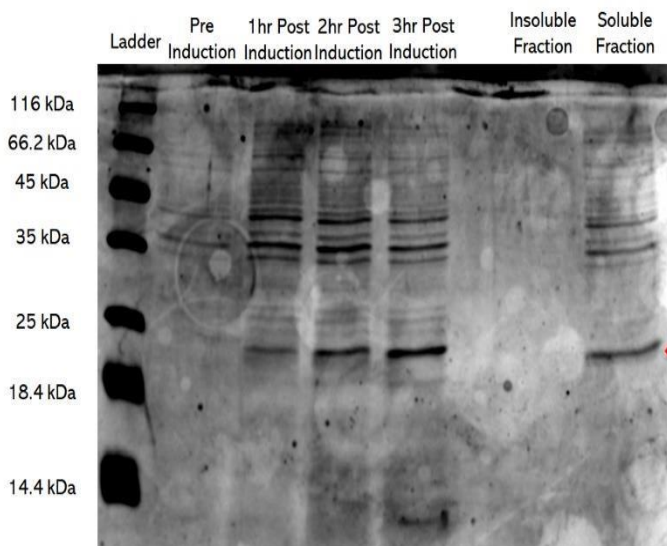
Figure 6: WT ParF Induction and Solubility

15% SDS-PAGE gel showing protein profile of 20 µL samples of transformant BL21 cells prior to and after induction with IPTG. The samples were taken immediately before and at hour long intervals after induction. Solubility test samples were 20 µL samples from the respective fractions of the culture following solubility assay. The molecular mass of ParF is labelled with the red arrow.

The purification of ParF was also performed successfully. The Bradford assay showed presence of protein in the fourth through eighth fractions, peaking at the sixth. An SDS-gel (Figure 7) was run to visualise fractions 3 through 8 as well as the flowthroughs from the purification. Figure 7 also showed a significantly higher amount of contaminating protein in

fractions 5 and 6 than would be expected, represented by a series of very thin bands and one thicker band around 35 kDa. The thick band is unlikely to be a dimer form of ParF as it is not of correct molecular weight. The 35 kDa band was present in a small capacity in the binding buffer flowthrough but was not visible in the wash buffer flowthrough. This contamination meant that fractions 5 and 6 would not be adequate for use in crosslinking experiments due to the potential for cysteine containing proteins to confound the results with false positives so were discarded. Contamination also meant that the concentration measurements of ParF gained from the Bradford assay were likely to be artificially increased by the presence of extra proteins (Figure 7).

Following this purification, the fractions were buffer exchanged by using a desalting column into storage buffer and frozen. However, this sample was rendered unusable due to the presence of DTT in the storage buffer, which would prevent interaction between cysteines and the BMOE crosslinker so the process was repeated using the same protocol with a final storage buffer not containing DTT (60).

Figure 7: WT ParF Elution Fractions

15% SDS-PAGE gel showing protein profile of 20 μL samples of sequential fractions eluted from wild-type ParF expressing cells following overexpression and Nickel tandem purification. The molecular mass of ParF monomers is labelled with the red arrow.

The second purification of WT ParF showed a significantly different elution pattern. This time, a proportion of ParF was visible in the insoluble fraction. The significant reduction in band intensity of the WT ParF band following the circulation on the resin denotes that the protein has adhered to the resin. The only band at around 14.4 kDa is most likely to be remnants of the lysozyme added during the early stages of the purification process (Figure 8a).

The ParF protein began to elute in the wash buffer. This was not the expected fraction for elution, though the lack of any other significant bands makes these samples equally as viable for use as an intended elution fraction, though the volume of 10 mL rather than 1.5 mL may have resulted in some dilution, obscuring the concentration when compared to the concentration present in the elution fractions (Figure 8b).

The elution fractions also showed WT ParF with very little visible contaminating protein, though the protein eluted much earlier than was the case in the previous purification. There is no clear reason for this earlier elution as the concentration of imidazole in the buffers was unchanged. Despite this, fractions 3 and 4 containing purified WT ParF were dialysed into storage buffer, Bradford tested and flash frozen for later use (Figure 8b).
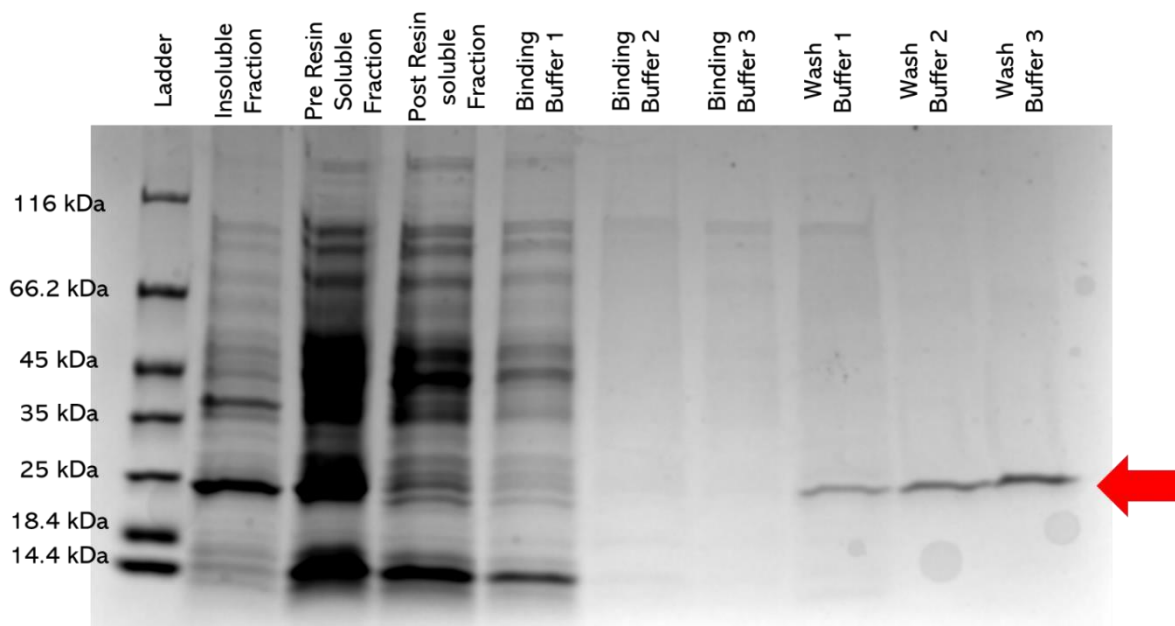
Figure 8a: WT ParF Elution Fractions

15% SDS-PAGE gel showing protein profile of 20 µL samples of initial fractions from TAP purification of WT ParF transformant cells following overexpression. The molecular mass of ParF monomers is labelled with the red arrow.
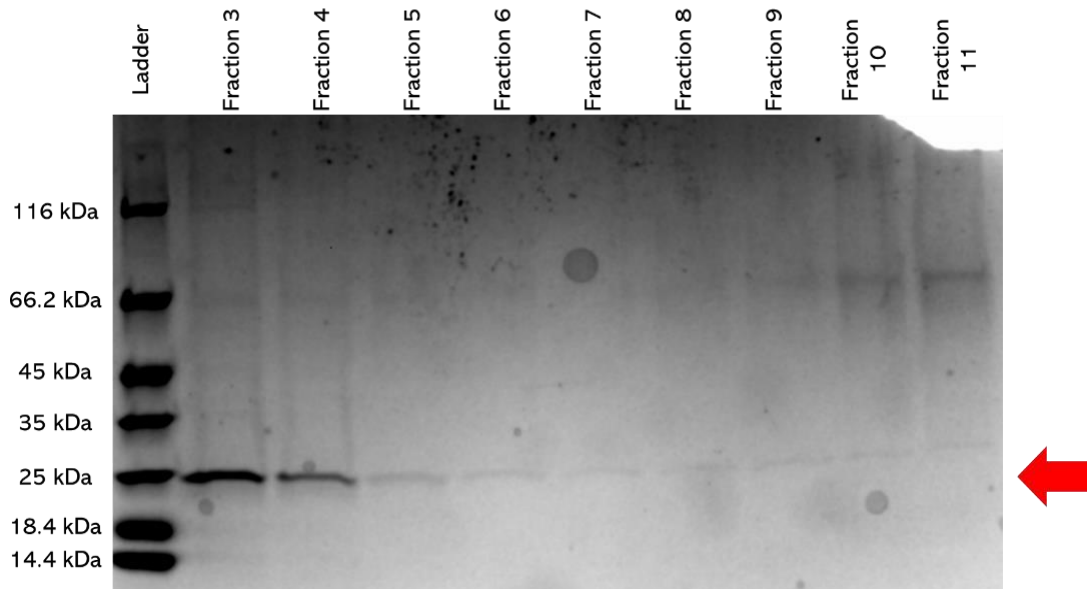
Figure 8b: WT ParF Elution Fractions

15% SDS-PAGE gel showing protein profile of 20 µL samples of fractions from TAP purification of WT ParF transformant cells following overexpression. The molecular mass of ParF monomers is labelled with the red arrow.

3.2.2 WT ParG

The WT ParG solubility analysis gel showed a strong increase of a band at slightly below 14.4 kDa, the expected weight of WT ParG, over the course of the three hours of induction (Figure 9). This was the only band that showed an increase in size and was also absent in the pre-induction sample. These data seem to show successful induction of the ParG protein.

Figure 9 showed some thick bands at 35 and 45 kDa. These bands were present over the course of the induction much as in the WT ParF gels. The WT ParG protein bands, though clearly present, were more diffuse than several of the heavier bands, which could imply a less successful induction than anticipated. Though as this occurs for all bands in this below 35 kDa in weight, it is more likely that this implies a technical issue with the gel running materials or process rather than a failure in overexpression of the protein. Fortunately, the visible bands at slightly under 14 kDa in the solubility test clearly show a more intense band in the soluble fraction over the insoluble fraction, which does not have any visible band at this weight at all. These data suggest that the ParG protein is both induced and is significantly more soluble than insoluble, allowing for purification steps to begin (Figure 9).
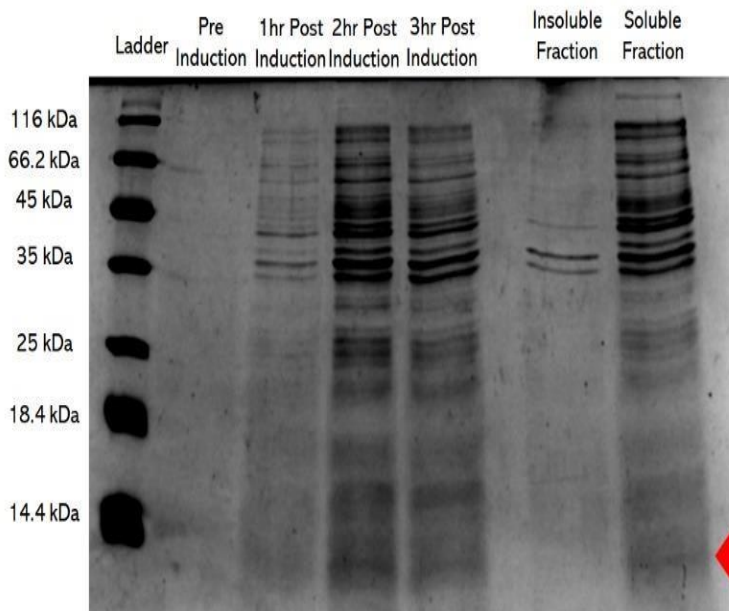
Figure 9: WT ParG Induction and Solubility

15% SDS-PAGE gel showing protein profile of 20 µL samples of transformant cells prior to and after induction with IPTG. The samples were taken immediately before and at hour long intervals after induction. Solubility test fractions were 20 µL samples from the respective fractions of the culture following solubility assay. The molecular mass of ParG monomers is labelled with the red arrow.

The following purification of ParG was successful, the fractions were all analysed by Bradford assay and fractions 3-8 showed presence of protein (Figure 10b). Samples of these fractions were analysed for purity on an SDS-gel which showed both intense bands at the expected molecular weight and no noticeable contamination from other proteins.

The analysis of the buffer flow-through fractions demonstrates several points (Figure 10a). It reaffirms the solubility of the ParG as the ParG band is considerably thicker in the pre-flow soluble fraction than in the crude pellet fractions to the point that the crude pellet band is almost totally absent. This same very thick band of ParG is also absent in the supernatant post-flow, which demonstrates that ParG has successfully bound to the resin in the column. The binding buffer flowthrough shows a small amount of residual protein, likely from the small volume of crude supernatant left in the column. The wash buffer fraction showed a similar array of proteins to the binding buffer fraction, but with even fewer bands, likely due to their being washed out, but for the exception of a slightly thicker band above 14 kDa. It is worth noting that this is unlikely to be small amounts of WT ParG elution in the imidazole; although the band is of adequate weight to be a dimer of ParG, due to the consistent presence of the band throughout Figure 10b with no change between the pre-flow and post-flow supernatant fractions, this would indicate that it is a different, similarly sized protein.
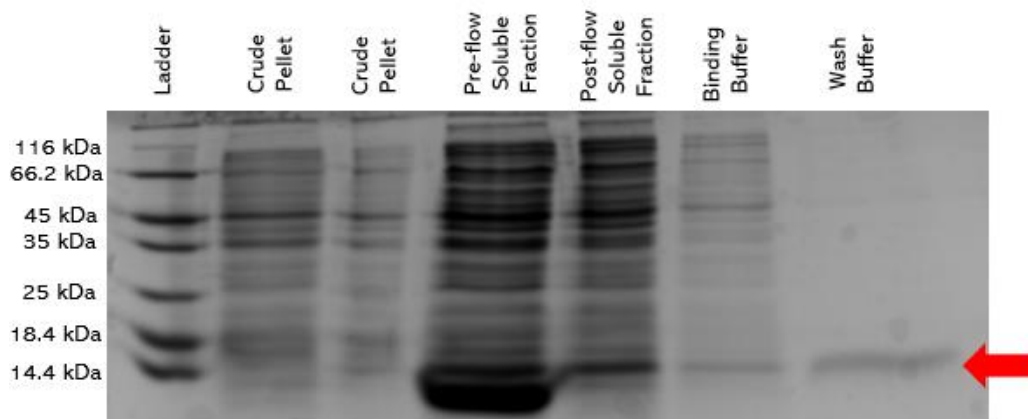
Figure 10a: WT ParG Elution Fractions

15% SDS-PAGE gel showing protein profile of 20 µL samples of initial fractions eluted from TAP purification of WT ParG transformant cells following overexpression. The molecular mass of ParG is labelled with the red arrow.
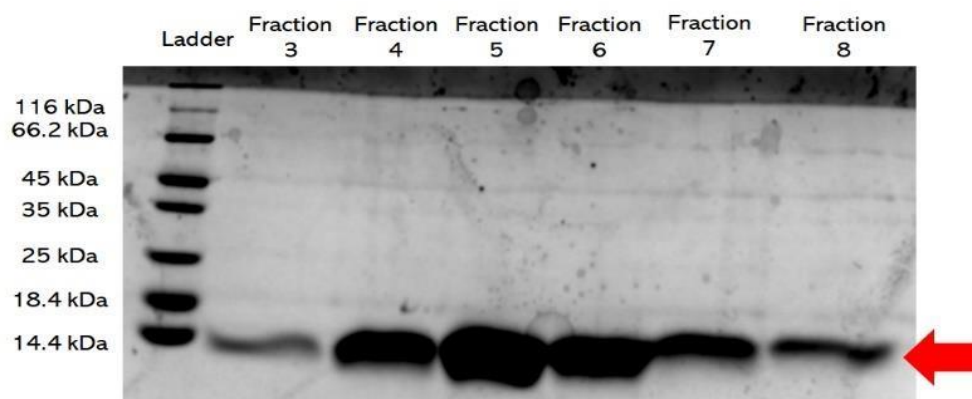
Figure 10b: WT ParG Elution Fractions

15% SDS-PAGE gel showing protein profile of 20 µL of fractions taken from TAP purification following overexpression of WT ParG transformant cells. The molecular mass of ParG monomers is labelled with the red arrow.

Due to the aforementioned issues with DTT in the storage buffer, the collected protein needed to be discarded and a new purification was performed. As no issues had occurred in purifying the WT ParG proteins, the variable imidazole wash buffer method described in the methods section was not deemed necessary. In this new purification, when comparing ParG present in the pre-resin (before it was loaded onto the column) and post-resin (after it was loaded) supernatants, the intensity of the ParG band in the post-resin fraction did not show as significant a decrease as compared to its counterpart in the pre-resin band than occurred in Figure 10a. This could imply that not all the protein was able to bind to the resin (Figure 11a).

The elution pattern of the protein was almost identical to the previous purification, but the amount of ParG in the elution fractions was less. The difference in band thickness in the pre-resin soluble fraction between purifications and lack of any noteworthy band at that

molecular weight would seem to indicate a lower level of ParG production in the sample overall; however, the band in the post-resin fraction is much thicker in Figure 11b than in Figure 10b. The data provided by comparison of these bands indicates that the protein production in the overexpression was less than that in the previous induction, but also that a smaller proportion of protein in this purification adhered to the gel. The most concentrated elution fractions were dialysed into storage buffer, measured for concentration, and then flash frozen.
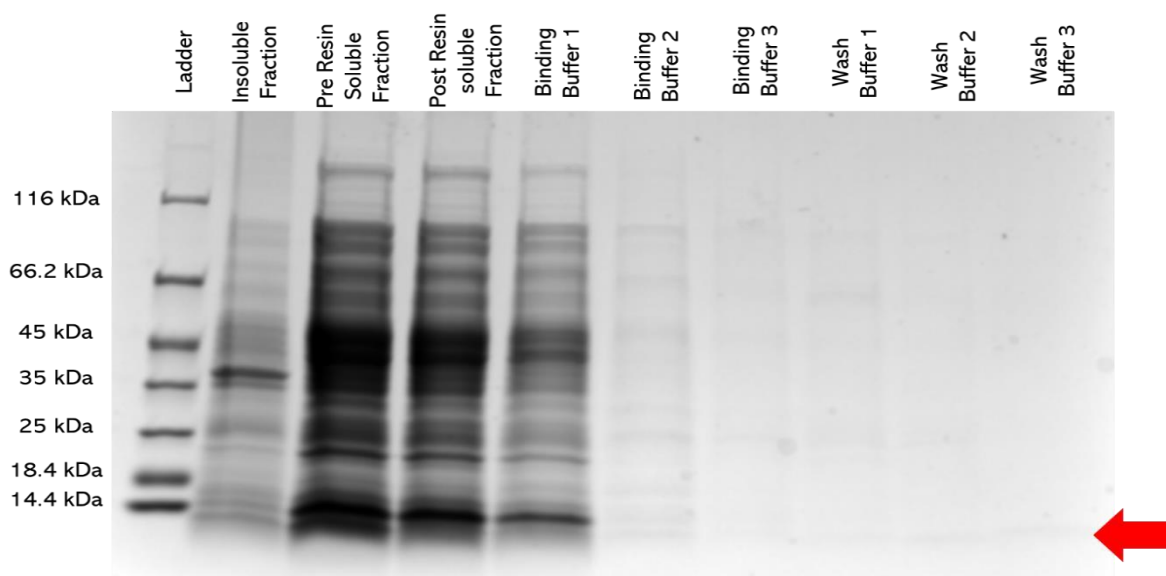
Figure 11a: WT ParG Elution Fractions

15% SDS-PAGE gel showing protein profile of 20 µL of fractions eluted from TAP purification following overexpression. The molecular mass of ParG monomers is labelled with the red arrow
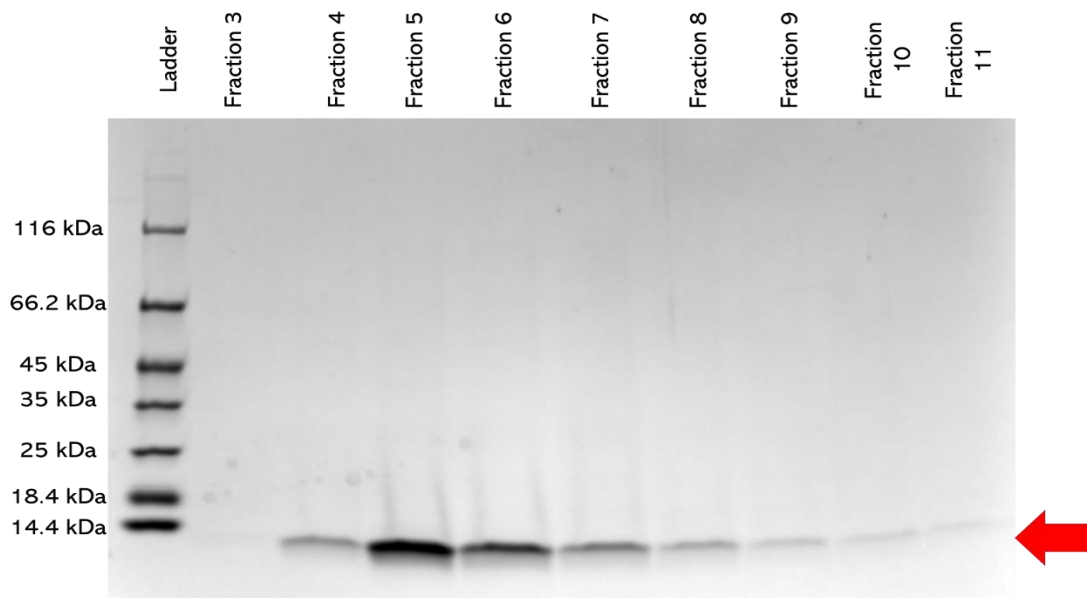
Figure 11b: WT ParG Elution Fractions

15% SDS-PAGE gel showing protein profile of 20 µL of fractions eluted from TAP purification following overexpression. The molecular mass of ParG monomers is labelled with the red arrow.

3.2.3 ParF-K155C

The solubility test of the ParF-K155C samples confirmed successful induction of the protein by IPTG as the weight of the 25 kDa bands, that indicate ParF-K155C protein, increased across the post-induction samples and were absent in the pre-induction sample. The solubility assay showed a significantly greater presence of ParF-K155C in the soluble fraction. The soluble fraction contained comparable bands to that of the 3-hour post-induction sample. The insoluble fraction does not show any insoluble ParF-155C protein but does show other protein. This led to the conclusion that there is a greater proportion of soluble ParF-K155C than insoluble and that it would be possible to purify (Figure 12).
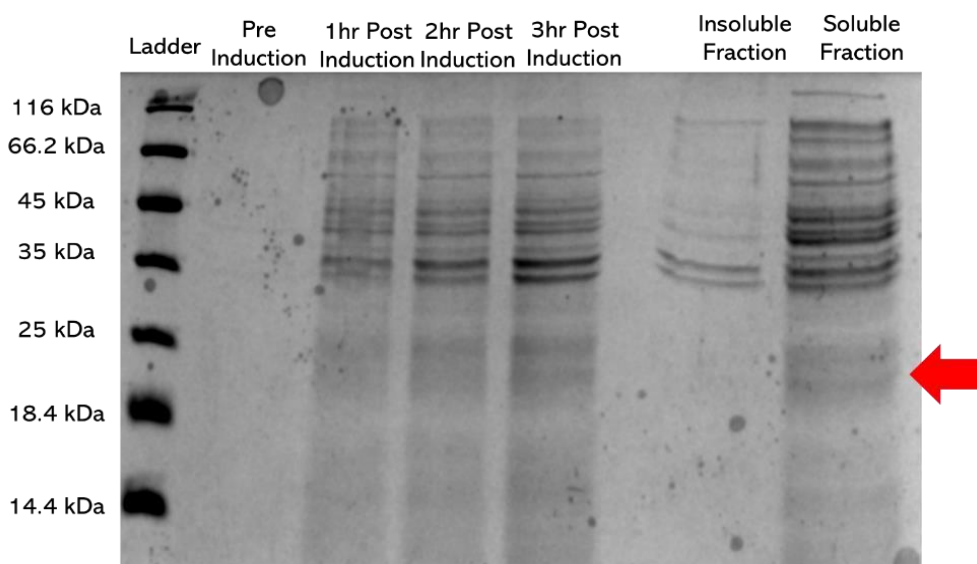
Figure 12: ParF-K155C Induction and Solubility

15% SDS-PAGE gel showing protein profile of 20 µL samples of transformant cells prior to and after induction with IPTG. The samples were taken immediately before and at hour long intervals after induction. Solubility test samples were 20 µL samples from the respective fractions of the culture following solubility assay. The molecular mass of ParF monomers is labelled with the red arrow.

A 300 mL liquid culture overproducing ParF-K155C was induced and the protein was purified via affinity column purification. Unfortunately, there were several failed attempts to purify the fractions due to various factors including contamination with incidental proteins and the mistaken addition of DTT in a way that would prevent crosslinking. Following the failed purifications, a further purification was done with the adjustment of the three separate wash and elution fractions as detailed in the methods section, resulting in a more successful purification. The SDS-gel showed presence of ParF-K155C in the insoluble fraction but a larger amount in the soluble fraction. Despite smudging, there was a clear decrease in the ParF-K155C protein in the post-resin fraction (Figure 13). These data indicated both a significant amount of protein produced and that a large amount of the ParF-K155C protein adhered to the resin. In considering the contaminants, the heavier bands show reduction following resin treatment, but there are no visible bands of this size anywhere other than the first binding buffer flowthrough. The ParF-K155C protein eluted much earlier than it had in previous purifications, showing a weaker binding to the resin, when compared with the WT ParF elution and providing further evidence for the C155 residue of the mutant affected protein binding. (Figures 9a, 9b, 13a, 13b).

The late wash buffer fractions and early elution buffer fractions were deemed pure enough for crosslinking and were dialysed into storage buffer and flash-frozen.
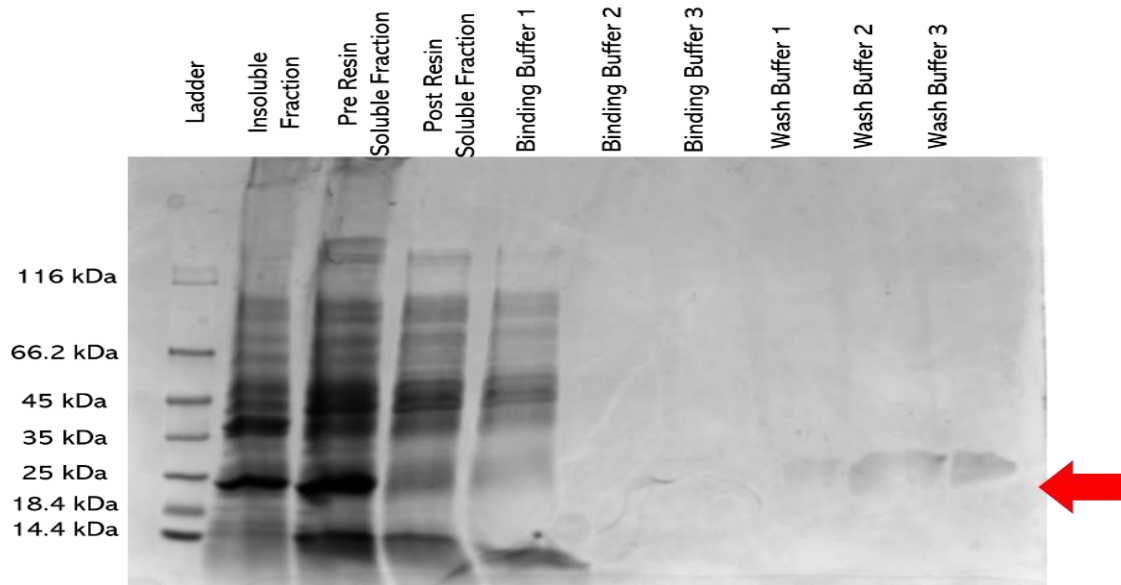
Figure 13a: ParF-K155C Elution Fractions

15% SDS-PAGE gel showing protein profile of 20 µL of sequential fractions eluted from the cell lysate of ParF-K155C expressing BL21 cells following column purification. Red arrow denotes the expected band weight of ParF monomers.
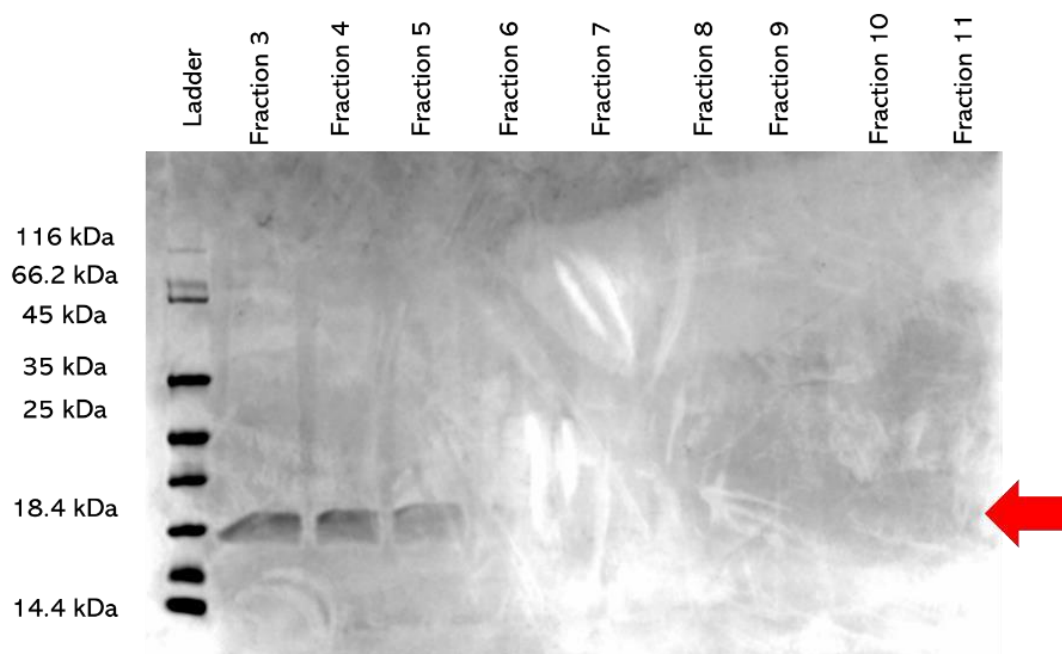
Figure 13b: ParF-K155C Elution Fractions

15% SDS-PAGE gel showing protein profile of 20 µL of sequential fractions eluted from the cell lysate of ParF-K155C expressing BL21 cells following column purification. Red arrow denotes the expected band weight of ParF monomers.

3.2.4 ParF-K160C

The gel image of the proteins purified from the initial overexpression of ParF-K160C showed a clear increase in global protein production following induction. This fits the expected induction pattern. The solubility assay showed a thicker ParF-K160C band in the of ParF-K160C (Figure 14).
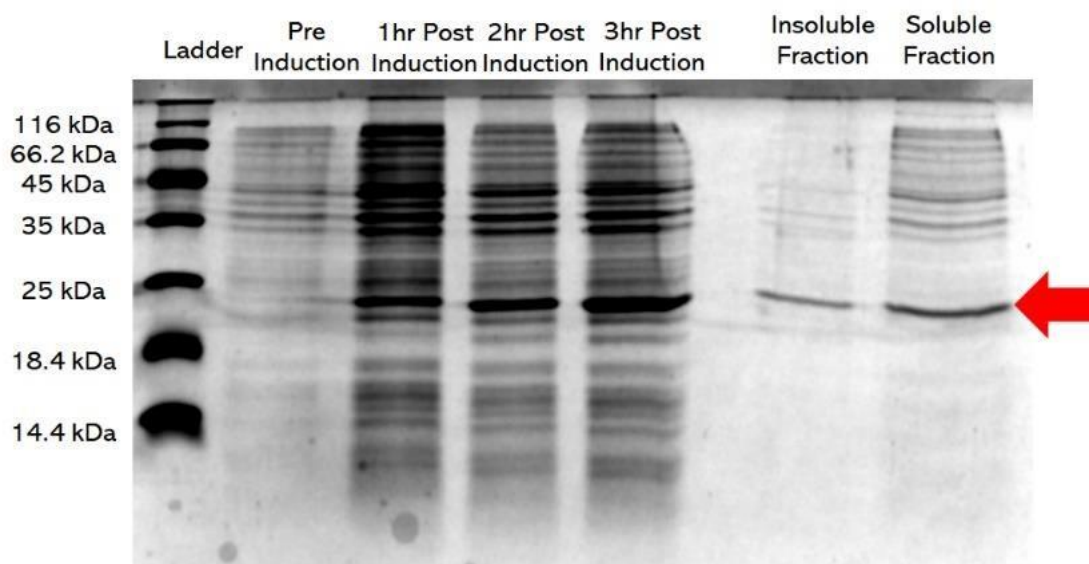
Figure 14: ParF-K160C Induction and Solubility

15% SDS-PAGE gel showing protein profile of 20 μL of samples of transformant cells prior to and after induction with IPTG. The samples were taken immediately before and at hour long intervals after induction. Solubility test samples were 20 μL samples from the respective fractions of the culture following solubility assay. The molecular mass of ParF monomers is labelled with the red arrow.

This purification of ParF-K160C was completed with the adjusted ParF purification procedure and the eluted protein fractions were dialysed against DTT-free storage buffer as detailed in the materials and methods section.

The initial results of the purification are clear and seem to be concomitant with the final ParF-K155C purification. The ParF-K160C band in the insoluble sample was significantly less intense than that in the soluble fraction, implying not only a much greater proportion available for purification, but the increased intensity of the band implied a higher amount of available protein as well. The reduction in intensity from the ParF-K160C band following circulation on the resin also suggested a very strong adherence to the resin. Especially compared to the other bands in these fractions, which were not being proportionally reduced by as much, indicating that the ParF-K160C was adhering much more strongly than any other protein, as expected (Figure 15a).

A 14.4 kDa protein is visible in all soluble fractions and in all binding buffers and in the first two wash buffers flow-throughs. This protein could be the lysozyme used to break the cell during extract preparation though this cannot be confirmed. (Figure 15a).

The elution of the ParF-K160C occurred very early on compared to its wild-type form, similarly to the Par-K155C purifications but with a different elution profile. The ParF-K160C eluted with almost equal band weight over more elution fractions without a notable increase or decrease in protein amount between wash buffer 2 and elution fraction 6. Although the ParF-K155C did elute more in the wash buffer than the ParF-K160C did in its purification, ParF-K160C also eluted in more fractions (eleven in total) implying that although the C160 residue still affected the binding of the protein to the resin, the specific cause may have been different from what caused the weaker binding of the ParF-K155C mutant as indicated by the change in elution profile (Figures 13a, 13b, 15a, 15b).
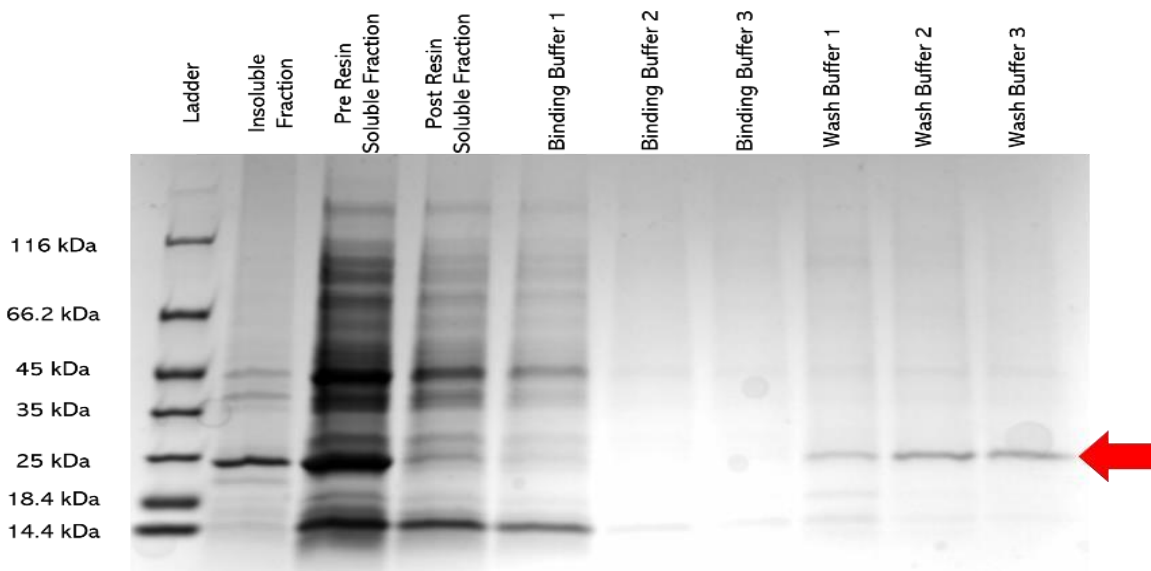
Figure 15a: ParF-K160C Elution Fractions

4-15% SDS-PAGE gel showing protein profile of 20 µL of fractions eluted from TAP purification following overexpression. The molecular mass of ParF monomers is labelled with the red arrow.
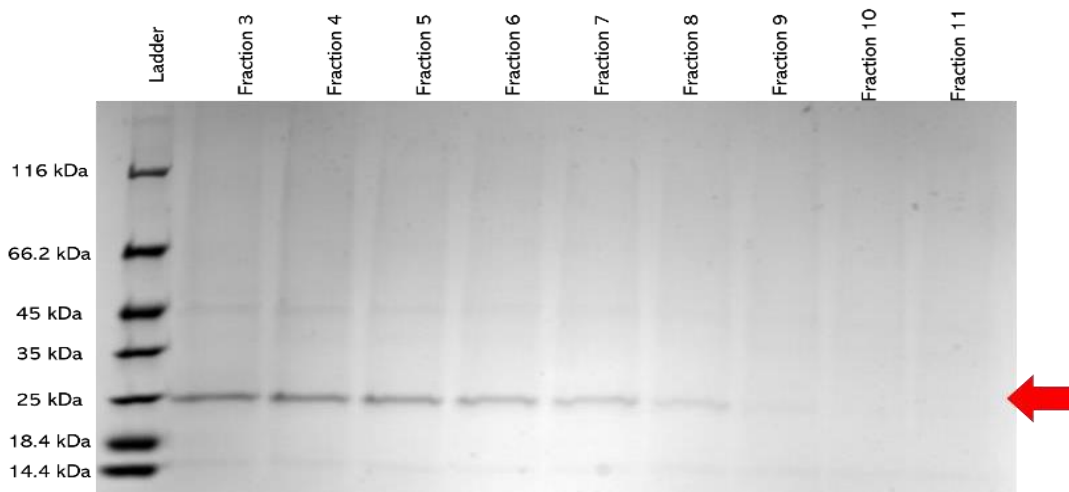
Figure 15b: ParF-K160C Elution Fractions

4-15% SDS-PAGE gel showing protein profile of 20 µL of fractions eluted from TAP purification following overexpression. The molecular mass of ParF monomers is labelled with the red arrow.

3.2.5 ParG-K11C

The induction of *parG*-K11C showed a successful production of protein just below 14.4 kDa, matching the expected molecular weight of ParG. This band increased in intensity over the first two hours of induction. Though there seemed to be a drop in expression level at three hours post-induction, there is still a significantly intense band of ParG-K11C protein. Solubility analysis confirmed that the protein was soluble. There was no visible band at the expected molecular mass of ParG-K11C in the insoluble fraction, but there were small bands at around 35 and 45 kDa consistent with the induced and uninduced fractions, giving credence to the conclusion that the representation of the insoluble fraction is accurate. This was convincing enough to pursue purification (Figure 16).
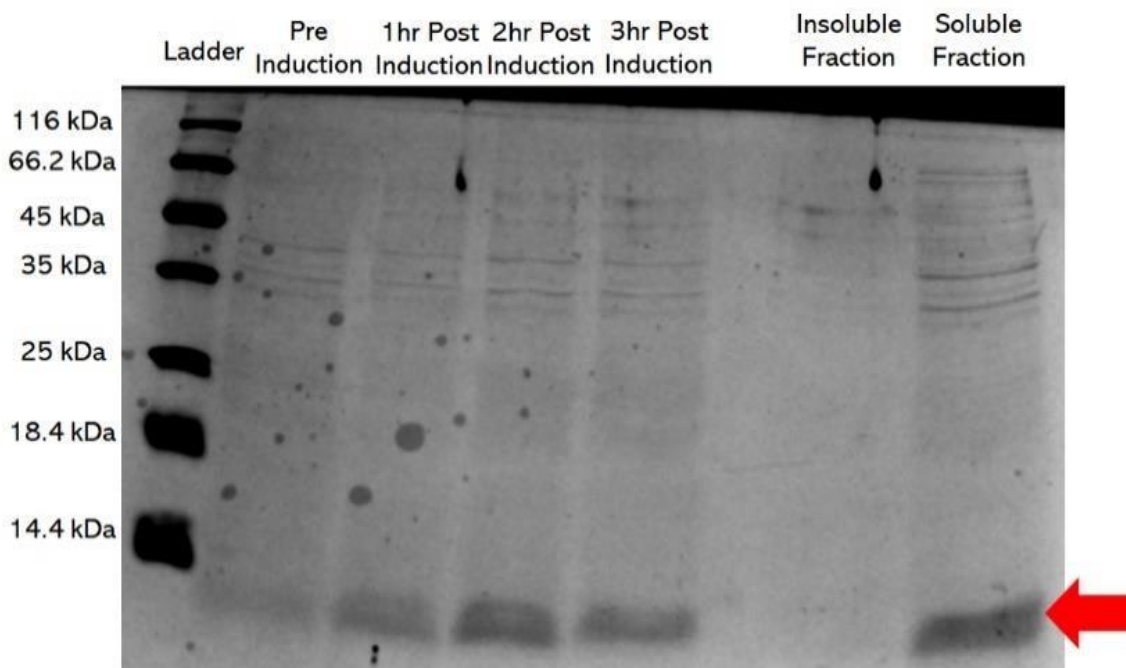
Figure 16: ParG-K11C Induction and Solubility

15% SDS-PAGE gel showing protein profile of 20 µL samples of transformant cells prior to and after induction with IPTG. The samples were taken immediately before and at hour long intervals after induction. Solubility test samples were 20 µL samples from the respective fractions of the culture following solubility assay. The molecular mass of ParG monomers is labelled with the red arrow.

Unfortunately, attempts to purify the protein using the column protocol were unsuccessful. Two separate attempts derived from different overproduction cultures both showed no visible amounts of protein of the eluted fractions on gels and were deemed insufficient to perform a crosslinking experiment. The lack of clear gel data means that it was not possible to accurately identify the issues with this purification and correct them.

Following the failure of the column purifications, a large-scale batch purification was attempted. This was intended to be a suitable alternative to the column, but it was not feasible as the proportion of liquid to soluble resin meant that a large proportion of the resin was lost at each step, leading to significant protein loss by the end of the process. Thus, the smaller scale batch purification protocol was adopted, as detailed in the methods section. This protocol reduced but did not eliminate the loss of resin at each step. However, despite initial proof that large-scale batch purification could be effective, attempts to scale down revealed that this method showed that it was not reliable in giving pure protein so was abandoned in favour of the altered TAP affinity protocol detailed in the materials and methods section.

The later attempt at purification of ParG-K11C indicates both that the ParG-K11C was soluble and that it adhered successfully to the resin. The contaminant bands at 35 and 45 kDa are present with increasing intensity in the wash buffer fractions and don't decrease until elution buffer fraction 7 (Figure 17). There were no significant contamination bands in the eluted samples but there was a broad smudge of bands higher up. As these bands were significantly thinner and less dense than the ParG-K11C bands, the samples were dialysed, subjected to Bradford assay and flash frozen in 200 µL aliquots. The storage buffer used in the dialysis of this purification used 30% glycerol to increase the concentration of the protein (61).
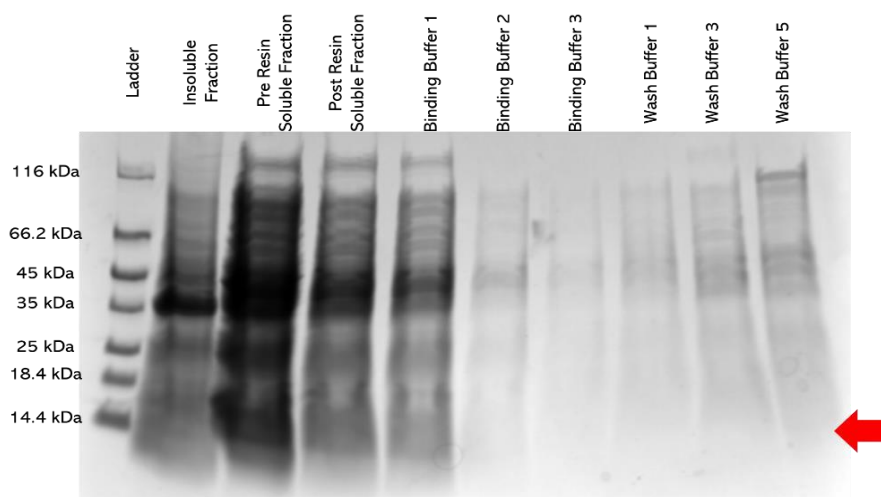
Figure 17a: ParG-K11C Elution Fractions

4-15% SDS-PAGE gel showing protein profile of 20 µL samples of fractions eluted from TAP purification following overexpression. The molecular mass of ParG monomers is labelled with the red arrow.

Figure 17b: ParG-K11C Elution Fractions

4-15% SDS-PAGE gel showing protein profile of of 20 µL samples of fractions eluted from TAP purification following overexpression. The molecular mass of ParG is labelled with the red arrow
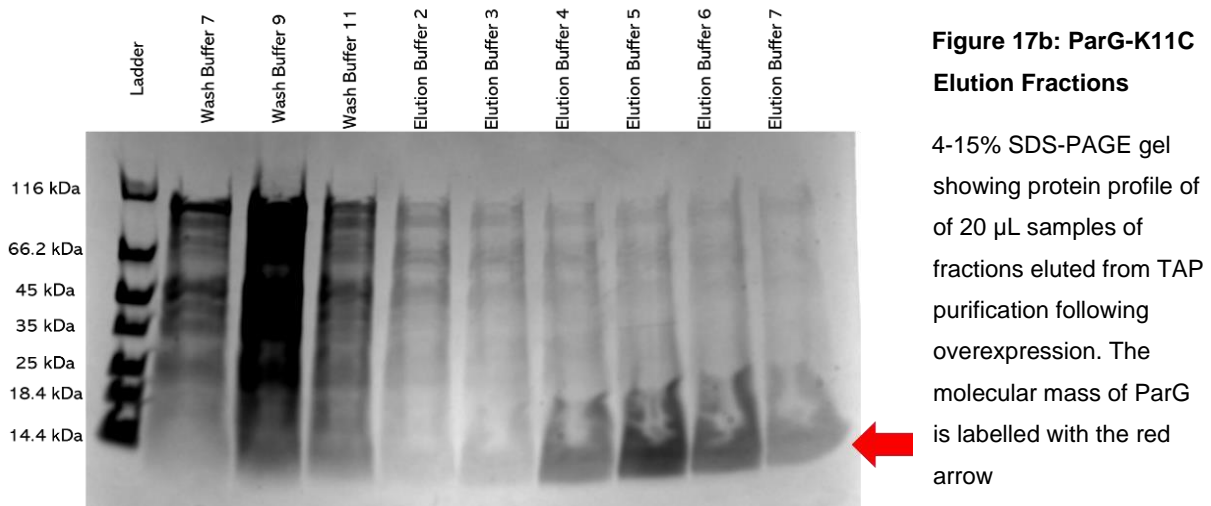
3.2.6 ParG-K12C

DNA extraction of the parG-K12C containing plasmid proved challenging. Following multiple attempts, it was not possible to produce a sample with a DNA concentration above around 5 ng µL^{-1}. This was corrected by making multiple purifications from a 40 mL liquid culture inoculated with a single colony and the DNA was eluted with water rather than AE Elution Buffer. These purifications were then concentrated in a Savant DNA Speed Vac DNA110 concentrator until their volume had decreased by around half, at which point they were pooled together and further concentrated. This was repeated until the concentration of the combined sample reached 127 ng µL^{-1} and the sample could be sent for sequencing.

The initial pilot induction demonstrated a substantial increase in the ParG-K12C protein amount over the course of the induction, showing that ParG-K12C was being successfully induced. The results of the solubility study showed a stronger band in the insoluble sample than the soluble sample. This result seemed to indicate that the mutation was causing the protein to aggregate (Figure 18).
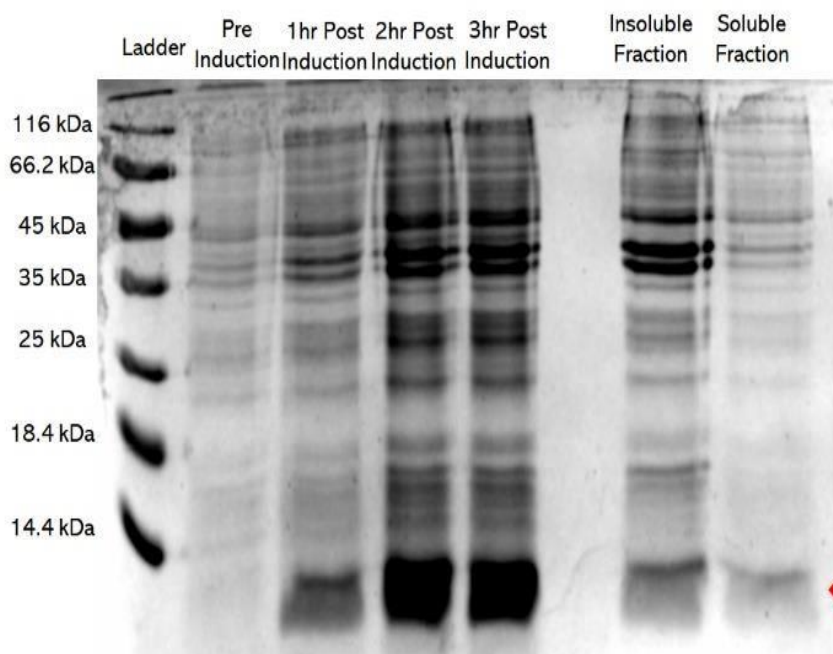
Figure 18: ParG-K12C Induction and Solubility

15% SDS-PAGE gel showing protein profile of 20 μL samples of transformant cells prior to and after induction with IPTG. The samples were taken immediately before and at hour long intervals after induction. Solubility test samples were 20 μL samples from the respective fractions of the culture following solubility assay. The molecular mass of ParG monomers is labelled with the red arrow.

Although it is possible that the C12 residue might cause aggregation or that association with the cell membranes or chromosomal DNA might bring the protein into the insoluble fraction, a more feasible hypothesis was that excessive sonication caused the protein in the culture to aggregate, rendering it insoluble (62). It is also possible that the K12C replacement was causing a significant increase in the DNA interaction of the ParG-K12C mutant, causing it to adhere to the chromosome.

In order to eliminate the possibilities of a mistake in the gel running or sonication induced aggregation, an induction and solubility test were repeated but using only ten cycles of sonication. The gel from this sample, shown in Figure 19, also demonstrated successful induction. It also suggested a decrease in expression after three hours of induction as the ParG-K12C band was weaker in the 3hr post-induction sample than the 2hr post-induction sample with no comparative decrease in the rest of the induction profile in either lane. The solubility analysis confirmed not only that the ParG-K12C protein was present in the soluble fraction, but that all other cellular proteins were present in the culture were as well. This aligned better with all data collected thus far and allowed me to proceed in purifying the proteins from the cell-lysate supernatant, though reduced sonication had likely reduced the number of lysed cells and therefore reduced the total amount of ParG-K12C released into the culture to end up in the supernatant than in the previous purification (Figures 18, 19). All subsequent ParG-K12C purifications used ten rounds of sonication rather than the previously used twelve.
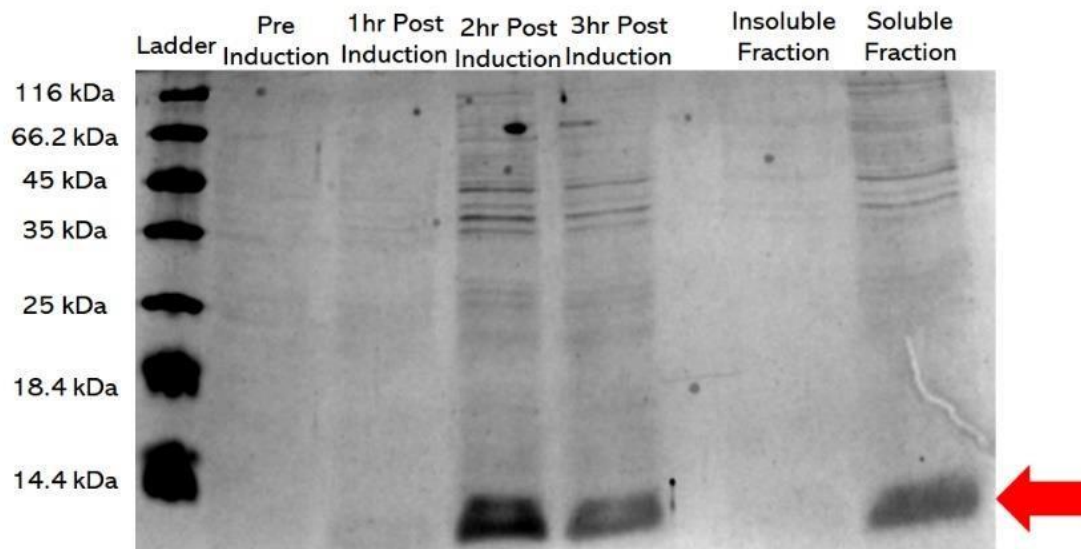
Figure 19: ParG-K12C Induction and Solubility

15% SDS-PAGE gel showing protein profile of 20 μL samples of transformant cells prior to and after induction with IPTG. The samples were taken immediately before and at hour long intervals after induction. Solubility test samples were 20 μL samples from the respective fractions of the same culture. The molecular mass of ParG monomers is labelled with the red arrow.

Unfortunately, initial attempts at purification were not successful. In performing a Bradford assay, only five of the fractions demonstrated any appreciable readings, all of which were below an OD595 of 0.015, implying very low protein concentration.

Following this failure to purify the ParG-K12C using the original method, despite evidence that the protein was soluble and did bind to the column, from this point the updated TAP affinity method was used to obtain samples of ParG-K12C as detailed in the methods section. The first purification did not show promising results early on due to the significant presence of unidentified contaminating proteins and no increase in solubility despite the reduced sonication. These elution fractions were deemed not suitable for cross-linking experiments and were discarded.

The next ParG-K12C purification was performed with fresh resin to prevent any potential contamination or damage from previous purifications, using the same protocol. The results from this purification showed an improvement: the SDS-gel showed a larger amount of soluble ParG-K12C and the proportion of mutant protein that bound to the resin was greater than in the previous purification of ParG-K12C (Figure 20a). There was also a comparatively weaker band in the first binding buffer fraction, also indicating higher amounts of binding to the resin. The significant band around 35 kDa also decreased following circulation on the resin, indicating some adhesion (Figure 20a).

There were no visible bands of any weight in any of the subsequent binding or wash buffer fractions. The low amount of mutant protein in the elution fractions suggests either a low level of adhesion to the resin or inability to elute the proteins from the resin (Figure 20b). The pattern of the ParG-K12C bands in the elution buffer being similar to the previous purifications suggests that it was a lack of proteins adhering rather than an aberration in the binding properties of the ParG-K12C. This protein was dialysed against storage buffer, but the Bradford assay showed that it was not of sufficient concentration to be used effectively in crosslinking experiments so was discarded.
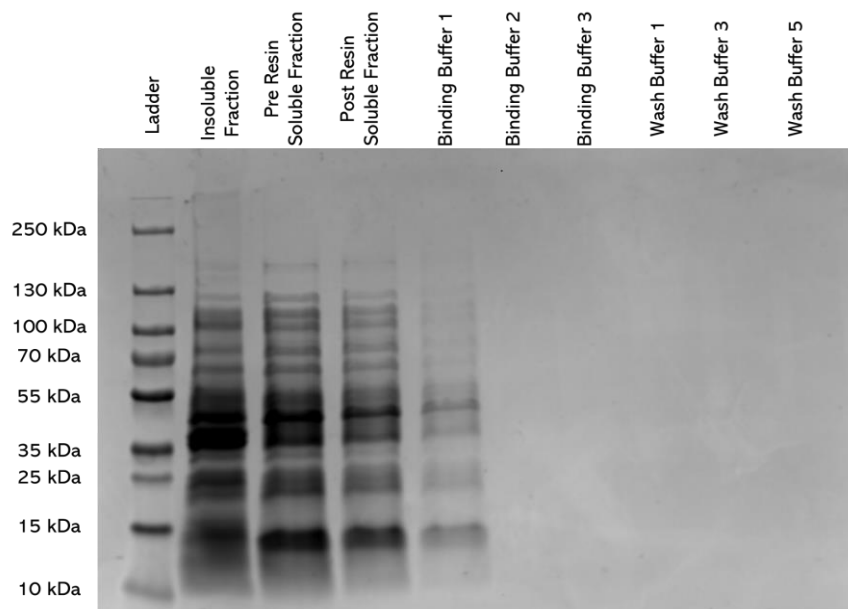
Figure 20a: ParG-K12C Elution Fractions

4-15% SDS-PAGE gel showing protein profile of 20 µL samples of fractions eluted from TAP purification following overexpression. The molecular mass of ParG monomers is labelled with the red arrow.
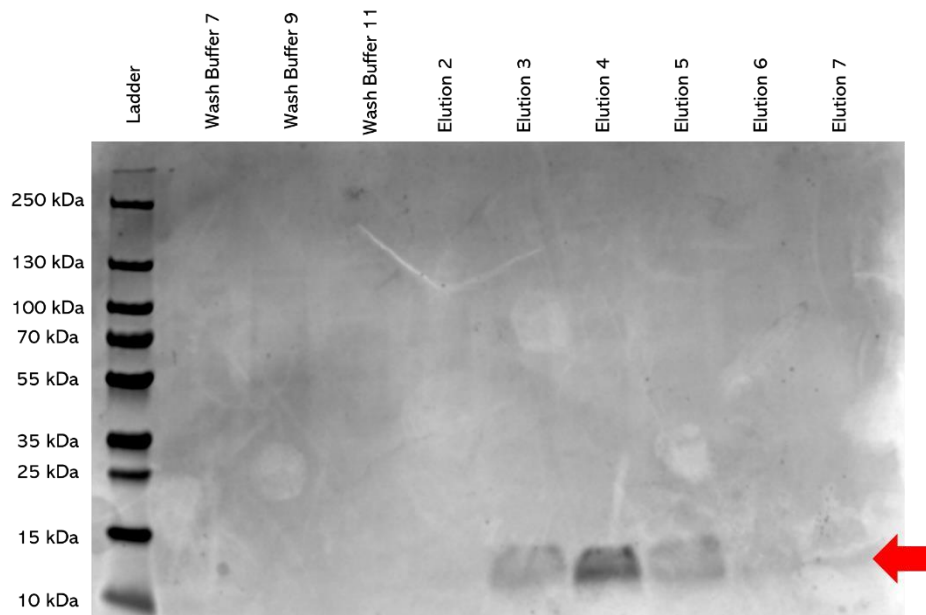
Figure 20b: ParG-K12C Elution Fractions

4-15% SDS-PAGE gel showing protein profile of 20 µL of fractions eluted from TAP purification following overexpression. The mass of ParG monomers is labelled with the red arrow.

A further purification, detailed in Figure 21, was performed according to the updated protocol detailed in the methods and materials section but was altered. Alterations consisted of by using an additional 2 mL of HIS binding resin in the column, 300 mL liquid culture's worth of frozen pellets rather than the usual 150 mL and the dialysis buffer included 30% glycerol rather than the usual 10%. These modifications were introduced to increase the concentration of the final sample as previous methods showed a limited effect in purifying the target protein.

The array of the bands in the interrogation fractions was very promising (Figure 21a). Though the insoluble ParG-K12C band was considerable, the amount of protein in the soluble fraction was greater. There was also an increased presence of the aforementioned 35 kDa and 45 kDa contaminant bands which promptly decreased in the post-resin soluble band, suggesting that they also adhered to the resin.

Wash buffer fractions 7 and 9 showed some unusual bands at 55, 70 and 130 kDa that persisted through the fourth elution buffer (Figure 21b). These bands have not been distinctly visible in any previous purifications. These proteins were probably present in the extracts used for previous purifications but they were more pronounced in this purification as a larger amount of cell pellet was used. These bands did not represent a significant contamination in any of the ParG-K12C elution flowthroughs.

The ParG-K12C bands in the elution fractions were unusually smudged, seemingly in contrast to all of the other bands present in the gels of this purification, though they eluted in a similar pattern to all previous ParG-K12C purifications and showed little contamination as mentioned above.

The fourth through seventh elution fractions were combined, dialysed against the 30% glycerol storage buffer and tested by Bradford assay. The average concentration across four tests in a Bradford assay showed concentration of 288 ng μL^{-1}, which was deemed adequate and the samples were aliquoted, flash-frozen and stored for use in crosslinking.
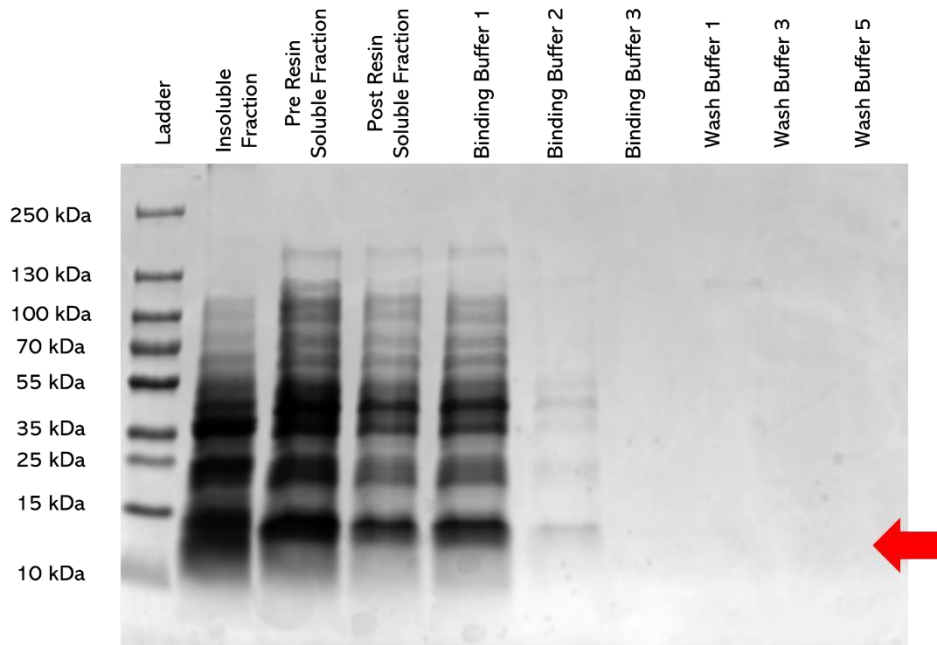
Figure 21a: ParG-K12C Elution Fractions

4-15% SDS-PAGE gel showing protein profile of 20 µL samples of fractions eluted from TAP purification following overexpression. The molecular mass of ParG monomers is labelled with the red arrow.
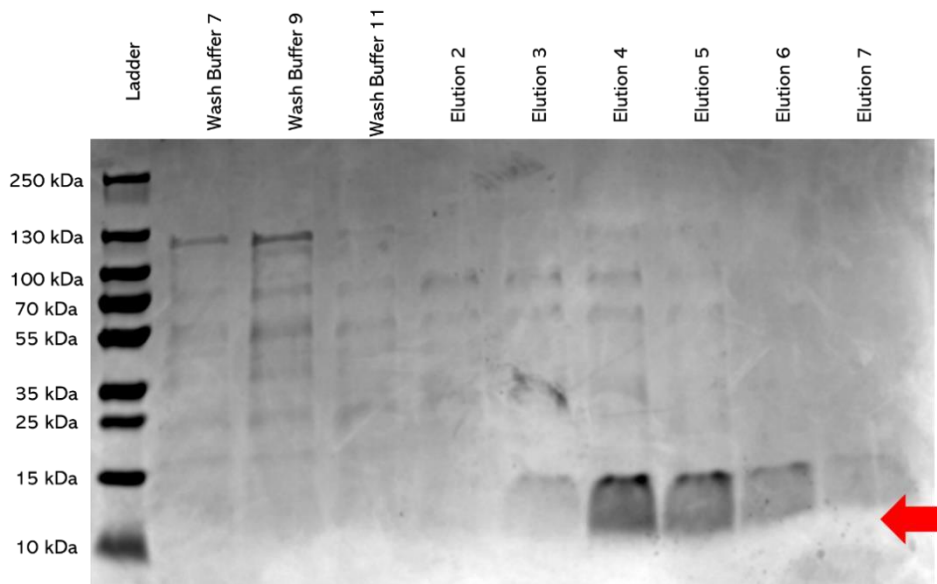
Figure 21b: ParG-K12C Elution Fractions

4-15% SDS-PAGE gel showing protein profile of 20 µL samples of fractions eluted from TAP purification following overexpression. The molecular mass of ParG monomers is labelled with the red arrow.

3.3 Crosslinking Assays

Once all proteins were successfully purified, multiple crosslinking experiments were performed using various protein concentrations to identify the best proportion of protein to be used in this assay. After some trials, it was decided to use a 10 µM sample of protein elution in each reaction to maximise clarity.

3.3.1 WT ParG – WT ParF

In the control crosslinking, there was only a small amount of WT ParF visible in lane 3 with no WT ParF visible in any other lane in the gel (Figure 22a). This precludes the use of either of these gels as an effective control for later treatment reactions' gels. The WT ParF from the same dialysis fraction showed a stronger presence on an earlier gel image (Figures 9 and 22). This shows that the protein has been lost following purification. This was most likely due to a failure in the procedure as it occurred in every lane that contained a sample of the WT ParF fraction.

The WT ParG protein was visible in all appropriate lanes across both gels. This also showed that the lack of WT ParF visible on the gels was not a failure in running the gels but in the ParF protein added. The majority of the WT ParG bands appeared as expected. There was no visible crosslinking with the WT ParF in lane 8 of the control gel or lanes 5, 7, 8 or 9 of the crosslinking gel and no indication of a change in molecular mass as a result of the ATP, MgCl2 or *parH*, as expected (42, 43, 63). Unfortunately, these gels also show an apparent crosslinking event in the BMOE reactions. (Figure 22).
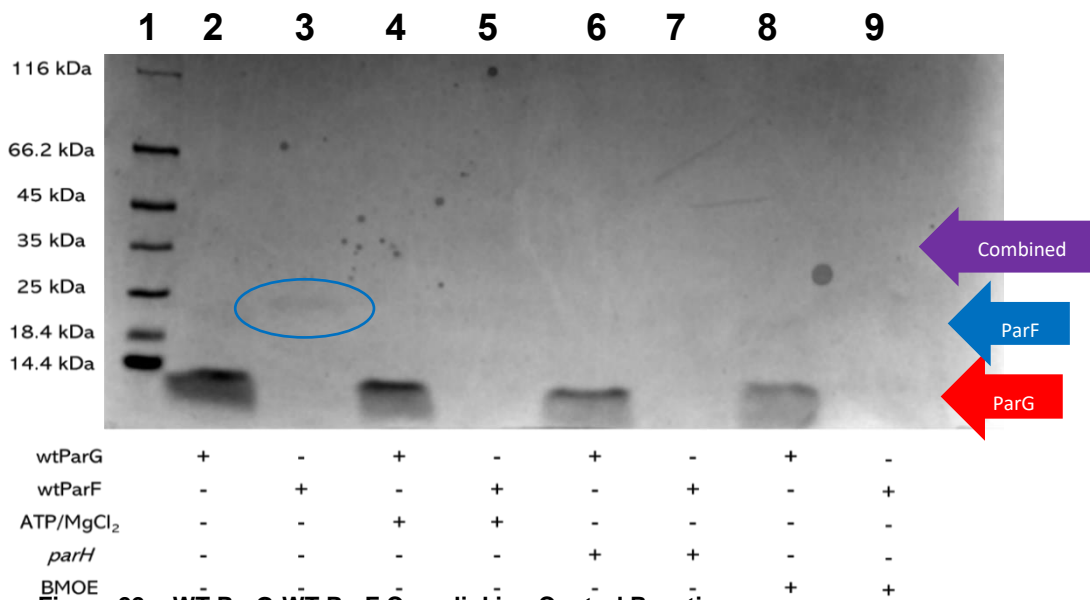
Figure 22a: WT ParG-WT ParF Crosslinking Control Reactions

4-15% SDS-PAGE gel showing protein profile of control crosslinking reactions consisting of one of WT ParG or WT Par F in conjunction with cofactor molecules and BMOE as detailed in section 2.2.2. **Legend**: + indicates the presence of the protein, cofactor or crosslinker in the reaction. – indicates it is absent in the reaction, the arrows show the expected mass of both proteins' monomers and of their combined mass. The ParF band in lane 3 is circled in blue for clarity
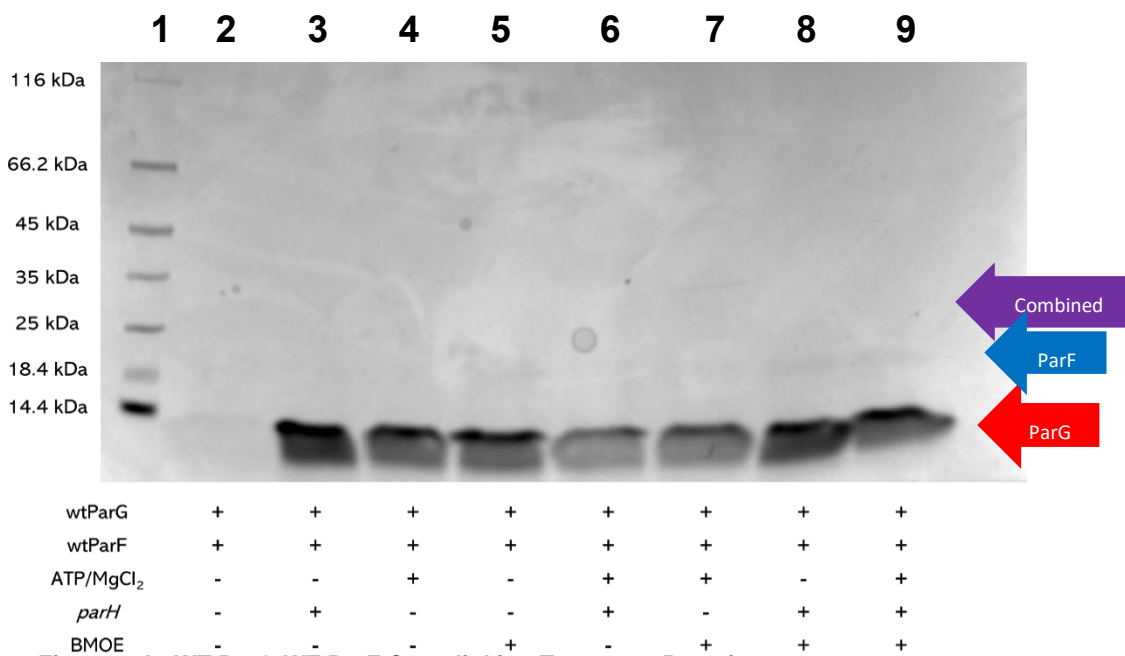
Figure 22b: WT ParG-WT ParF Crosslinking Treatment Reactions

4-15% SDS-PAGE gel showing protein profile of treatment crosslinking reactions containing both WT ParG and WT ParF in conjunction with cofactor molecules and BMOE crosslinker as detailed in section 2.2.2. **Legend**: + indicates the presence of the protein, cofactor or crosslinker in the reaction. – indicates it is absent in the reaction, the arrows show the expected mass of both proteins' monomers and of their combined mass.

3.3.2 ParG-K11C – ParF-K155C

The ParG-K11C and ParF-K155C mutants were incubated together in either presence or absence of the crosslinker BMOE in reaction mixtures containing other cofactors promoting complex formation. Unfortunately, the concentration of the ParF mutant proved insufficient to produce a discrete band visible on SDS-gel (Figure 23). Though there were very smeared bands in the ParF-K155C control reactions that did not match any in the ParG-K11C control reactions, none of them corresponded well to the sizes of any multimers of ParF-K155C. This led to the hypothesis that they are contaminants that are more visible due to the high concentration used to attempt visible protein bands. There were also thin bands present in the ParG-K11C control gel in lanes 2, 4, 6 and 8 that are not present elsewhere (Figure 23a). They do not match the ladder but do resemble the faint bands in the ParG-K11C-ATP/MgCl$_2$ and ParG-K11C - *parH* samples, several of which match with the sizes of ParG multimers, perhaps implying some oligomerisation (Figure 17). The ParG-K11C control samples show a consistent band at expected height, lane 4 had no visible change in the ParG-K11C band but lane 6 did, showing a less intense band (Figure 23). This confirms that the mutation did not entirely inhibit the binding of ParG-K11C to *parH*.
Lane 8 generated an unexpected result. If the ParG N-terminal flexible tails were interacting with one another in the dimer, we would expect to see a covalently crosslinked dimer band in the denaturing SDS-gel. However, Figure 23a showed not only the crosslinked homodimer band that occurred from the crosslinking of two ParG monomers, but a series of bands, decreasing in intensity with increasing mass after the 25 kDa band.

Each of the positions of the bands in this sample match with the expected mass of a ParG multimer, containing both odd and even numbers of monomers. The only possible cause is the C53 residue found in the C-terminal domain of the protein. This residue was, mistakenly, not initially considered in the experimental procedure. Lane 8 seemingly implies that both of the cysteines present in the ParG-K11C were crosslinking to cysteines on other ParG-K11C monomers. There were not sufficient contaminants to give bands of the intensity seen in Figure 23a so the protein is comprised solely of the more visible ParG-K11C. The bands with molecular weight greater than the dimers would be comprised of additional monomers of ParG-K11C that crosslinked through two available cysteine residues on two separate monomers, creating a chain, as modelled in Figure 24.
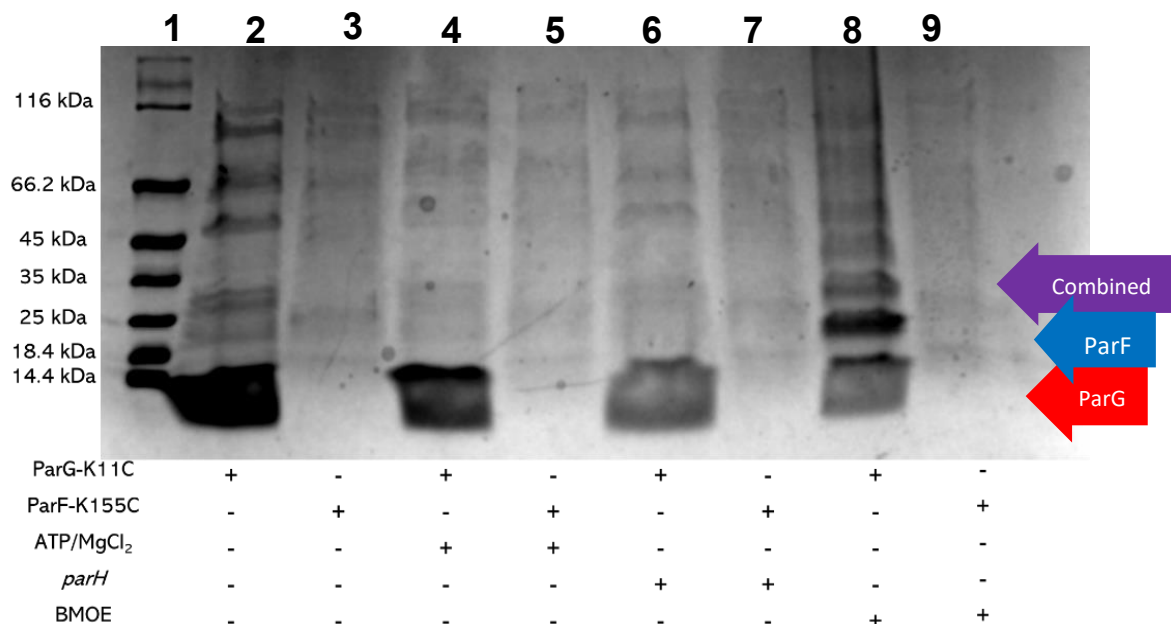
Figure 23a: ParG-K11C – ParF-K155C Crosslinking Control Reactions

	2	3	4	5	6	7	8	9
ParG-K11C	+	-	+	-	+	-	+	-
ParF-K155C	-	+	-	+	-	+	-	+
ATP/MgCl₂	-	-	+	+	-	-	-	-
parH	-	-	-	-	+	+	-	-
BMOE	-	-	-	-	-	-	+	+

4-15% SDS-PAGE gel showing protein of control crosslinking reactions consisting of one of ParG-K11C or ParF-K155C in conjunction with cofactor molecules and BMOE crosslinker as detailed in section 2.2.2. **Legend**: + indicates the presence of the protein, cofactor or crosslinker in the reaction. – indicates it is absent in the reaction, the arrows show the expected mass of both proteins' monomers and of their combined mass.

	2	3	4	5	6	7	8	9
ParG-K11C	+	+	+	+	+	+	+	+
ParF-K155C	+	+	+	+	+	+	+	+
ATP/MgCl₂	-	-	+	-	+	+	-	+
parH	-	+	-	-	+	-	+	+
BMOE	-	-	-	+	-	-	+	+
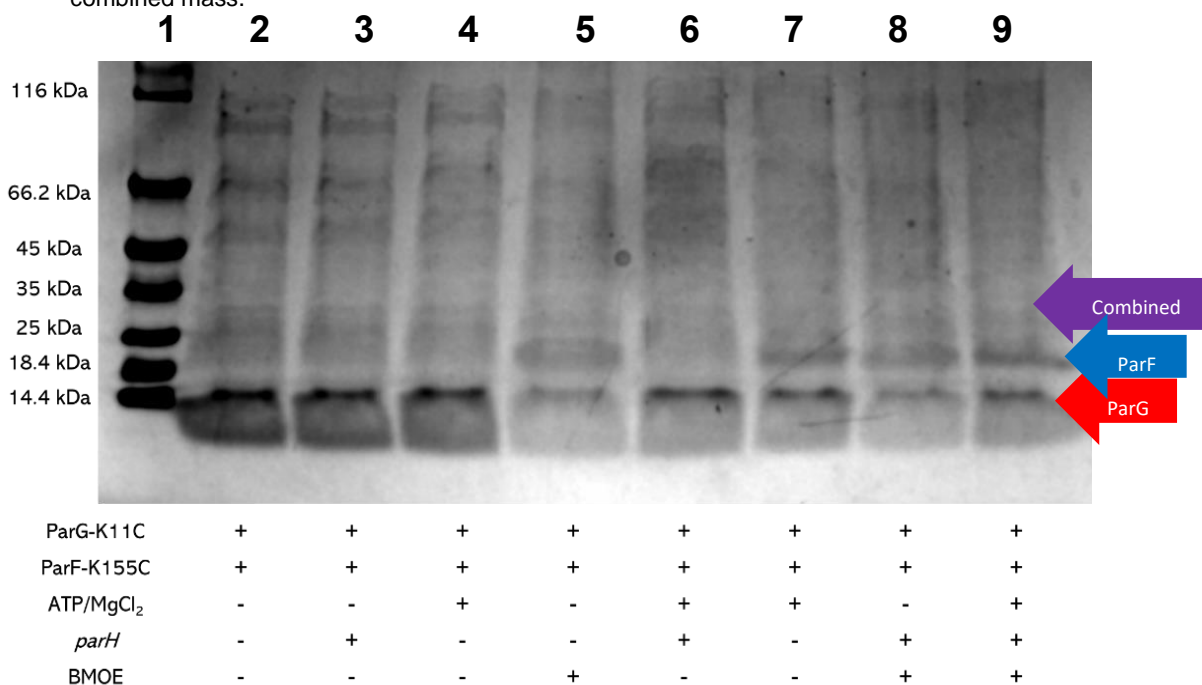
Figure 23b: ParG-K11C – ParF-K155C Crosslinking Treatment Reactions

4-15% SDS-PAGE gel showing protein profile of treatment crosslinking reactions consisting of both ParG-K11C and ParF-K155C in conjunction with cofactor molecules and BMOE crosslinker as detailed in section 2.2.2. **Legend**: + indicates the presence of the protein, cofactor or crosslinker in the reaction. – indicates it is absent in the reaction, the arrows show the expected mass of both proteins' monomers and of their combined mass

51
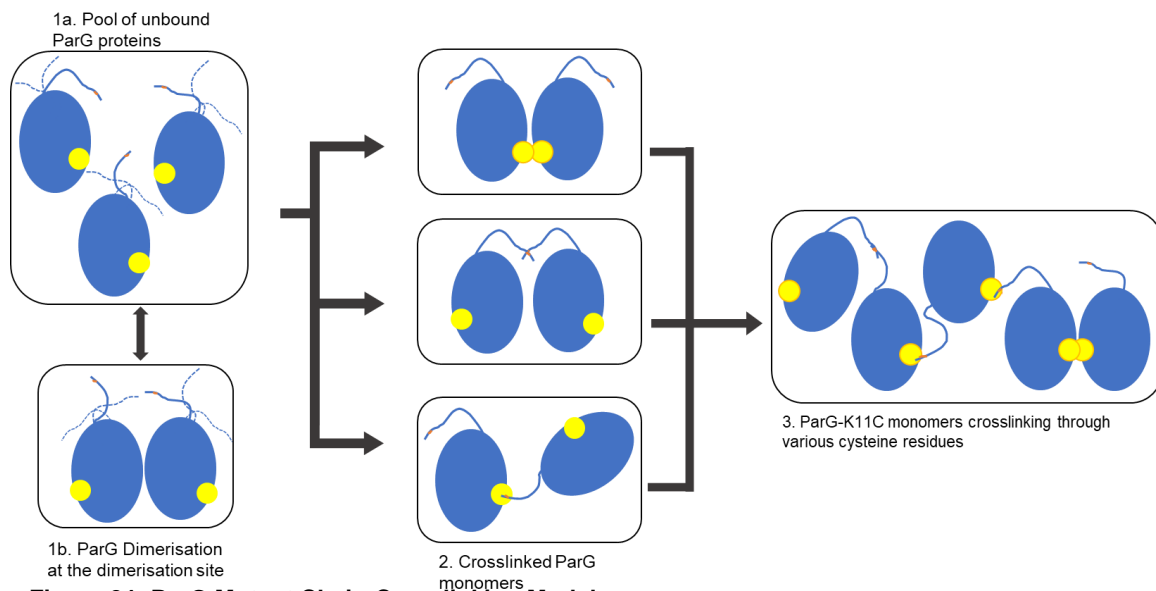
Figure 24: ParG Mutant Chain-Crosslinking Model

Cartoon showing proposed model for the crosslinking of mutant ParG proteins. Yellow denotes the C56 residue, orange denotes the K11C or K12C residue.

The treatment gel for the ParG-K11C - ParF-K155C contained some faint bands that match the expected weight of a ParF-K155C. Though they are very faint and are not visible in the control gels. These bands are not as strong as would be expected from the purification fraction, implying that the loss of visible ParF-K155C in these gels is occurring similarly to the WT ParF (Figures 11b and 23b). The loss of multiple different ParF samples following positive results imaged on gels indicates an issue in the mechanism used to store the ParF following purification. This issue is unique to the ParF protein because the ParG was unaffected despite identical treatment. Freezing and dialysis are the processes that occur after the gels that showed presence of ParF protein (Figure 11). The only issue that could occur in the dialysis that would only affect ParF is an inability to stay whole in the storage buffer, which is unlikely as it is chemically similar to the elution buffer which never generated damage even after several days. The conclusion from this data is that the reduction in ParF is being caused by the flash-freezing and storage of the ParF samples.

The ParG-K11C dimer bands in the treatment gel are less intense than the band in the control gel. This initially seem to indicate that the presence of ParF-K155C has an inhibitory effect on the crosslinking reaction of ParG-K11C, the reduction in band strength may be due to interaction between the two mutant proteins, which would be expected if the interaction site of ParG-K11C, the N-terminus is occupied interacting with a mutant of ParF and unable to be crosslinked into a dimer/multimer. Unfortunately, due to the reduced presence of visible ParF and low quality of the gels, it is not possible to conclude whether the reduction in band intensity was due to interaction of the proteins.

This is a difficult set of results to draw conclusions from as the presence of ParF-K155C is too weak to be visible regardless of the presence of BMOE, meaning that inferences must be made from the point of view of the ParG-K11C for the most part. This makes any conclusions that include ParF-K155C almost entirely speculative but the conclusions regarding the ParG-K11C are certainly that they are able to crosslink from two separate cysteine residues. This most likely occurs by crosslinking between monomers in the chainlike manner expressed in Figure 24. This crosslinking occurs with decreasing frequency and clarity on the gel images as the number of monomers added to the structure increases.

3.3.3 ParG-K11C – ParF-K160C

The ParG-K11C and ParF-K160C mutants were incubated together in either presence or absence of the crosslinker BMOE in reaction mixtures as detailed in the method section. The concentration of ParF-K160C was brought up to 13 µM in an attempt to improve visualisation on the gel for Figure 25. However, this resulted in the appearance of a significant contaminant in the lanes containing ParF-K160C. Additionally, there was band visible at the band mass of ParF-K160C. The contaminant protein migrated just above the position of the ParG-K11C bands at 14.4 kDa and is only visible in reactions containing the 13 µM samples of ParF-K160C. The only known protein this band could be is chicken egg white lysozyme. The weight of the protein is particularly easy to equate to the ladder as it is the protein used for the 14.4 kDa band of the ladder and appears at exactly the correct level in the gel as well as being a protein that was deliberately added to the solution as part of the protocol, explaining its presence at such a high proportion (64). Though it is worth noting that chicken egg white lysozyme contains cysteine so would likely show a reduction in band thickness in lane 9, which did not happen, making an unknown contamination more likely (65). It is also possible that the presence of this band and the absence of the ParF-K160C band could imply that the ParF-K160C proteins were cleaved into two pieces of almost identical mass by a method such as an unconsidered peptidase or overly intensive sonication.

Using the two equal contaminant bands as control bands to determine the behaviour of the thicker ParF-K160C band between purification and crosslinking, it appears that the ParF-K160C fraction is lost, rather than the other two becoming more concentrated as I initially hypothesised. The 45 kDa and contaminant band are both visible in the crosslinking control assay but only after the increase in concentration of the sample and neither seems to be proportionally different from the other, implying that they were not significantly affected by the dialysis and storage process. The ParF-K160C band, on the other hand, has been

reduced to almost nothing without affecting the other proteins in the solution. This did not visibly occur in any of the ParG purification fractions, implying that the loss of protein is occurring only in the ParF samples. This indicates that the ParF mutant is unstable in solution and tends to precipitate. The ParF-K160C bands are not visible and so the ability of the ParF-K160C protein to form covalent dimers in the presence of the BMOE crosslinked cannot be appreciated in these gels.

The ParG-K11C showed a series of bands at around 25, 50, 66 and just under 116 kDa in lanes 2, 4 and 6 that do not fit with the expected size of the protein or any multimer it would form. These reactions don't contain any BMOE so the bands aren't the result of any crosslinking and are also present in Figure 25b, meaning that they are contaminant proteins in the ParG sample. No additional bands appear that would indicate that these proteins crosslink with the ParG-K11C in lane 8 as any distinct bands fit the size of a potential multimer of ParG-K11C, allowing me to conclude that any crosslinking occurring is not sufficient to cause additional visible bands in the gel and therefore should not be considered to present an issue in reading the data from the gels.

The reactions containing BMOE in both gels demonstrate a similar set of results to the ParG-K11C and ParF-K155C reactions containing only a single protein in Figure 23b, represented by the presence of the same visible contaminant band and more well defined bands representing the ParG-K11C dimer and trimer bands before becoming less distinct after 35 kDa and possessing a smeared section above 116 kDa in BMOE containing reactions where reactions not containing BMOE did not. The ParG-K11C dimer band in Figure 25a is less intense than in Figure 23a, indicating that the crosslinking to form more dimers than monomers may not have been representative.

The implication is that the smear appears to indicate that the ParG-K11C or ParF-K160C mutants interacting with one other in the presence of BMOE. This would adequately explain the gap in the first few dimers as the binding of ParG to ParF is transient but becomes more frequent with the adherence of multiple dimers of ParG bound to DNA (*parH* in the case of the wild-type ParFG*H* system) in the same location.

Unfortunately, due to the high amount of visible contamination in the samples and low level of visible ParF-K160C, it is impossible to draw any definite conclusions about the nature of the smeared sections.
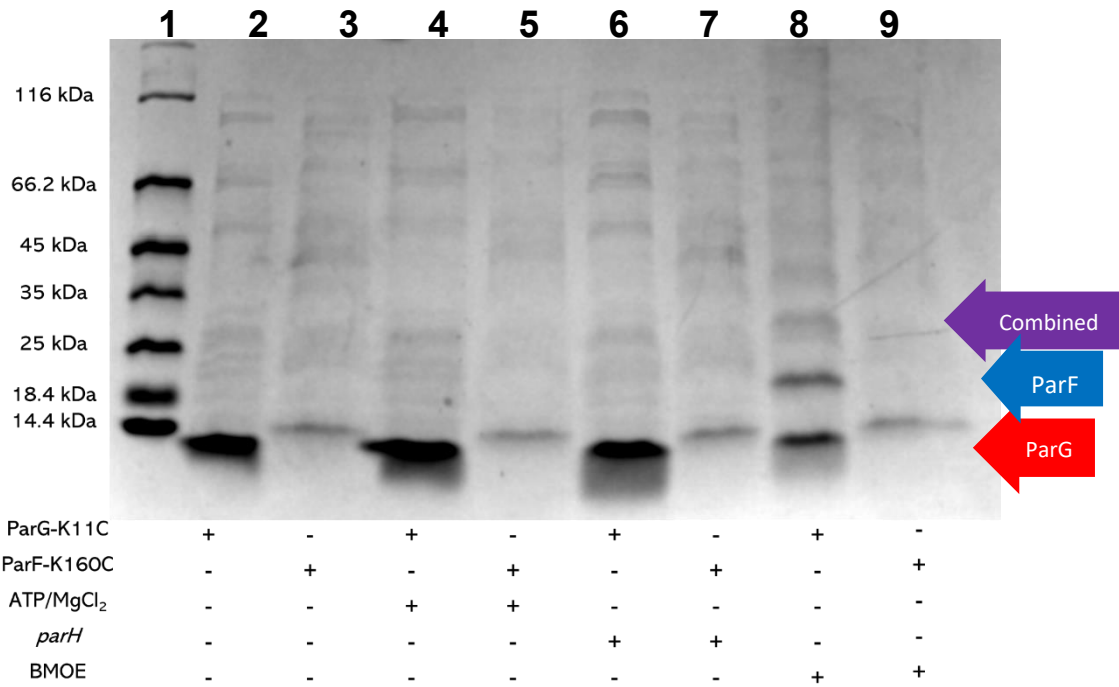
Figure 25a: ParG-K11C – ParF-K160C Crosslinking Control Reactions

4-15% SDS-PAGE gel showing protein profile of control crosslinking reactions consisting of one of ParG-K11C or ParF-K160C in conjunction with cofactor molecules and BMOE crosslinker as detailed in section 2.2.2. **Legend**: + indicates the presence of the protein, cofactor or crosslinker in the reaction. – indicates it is absent in the reaction, the arrows show the expected mass of both proteins' monomers and of their combined mass.
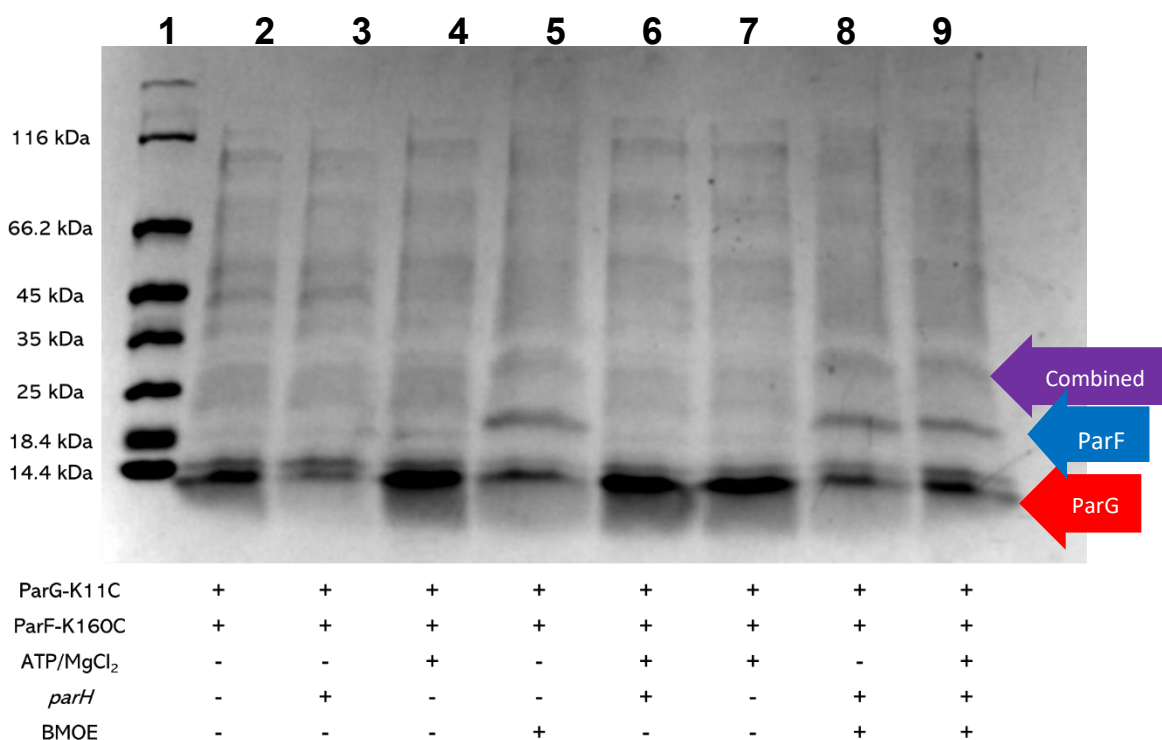
Figure 25b: ParG-K11C – ParF-K160C Crosslinking Treatment Reactions

4-15% SDS-PAGE gel showing protein profile of treatment crosslinking reactions consisting of both ParG-K11C and ParF-K160C in conjunction with cofactor molecules and BMOE crosslinker as detailed in section 2.2.2. **Legend**: + indicates the presence of the protein, cofactor or crosslinker in the reaction. – indicates it is absent in the reaction, the arrows show the expected mass of both proteins' monomers and of their combined mass

3.3.4 ParG-K12C – ParF-K155C

The initial crosslinking gels in the ParG-K12C - ParF-K160C also failed to run effectively and were discarded. Subsequent gels were more successful but did not display strong bands in most lanes. In these reactions the ParF concentration was increased to 13 µM to attempt better visualisation of the ParF-K155C protein.

The initial bands of ParG in lanes 2, 4 and 6 were broadly similar to those observed in other crosslinking reaction gels, though some more distinct bands in the ParG-K12C controls were visible. The majority of which do not align with the expected masses of ParG-K12C multimers and are likely to be contaminating proteins (Figure 26a).

Of the visible bands in lane 8 of Figure 26a, the monomer band is the strongest, albeit significantly weaker than the same band in the other control reactions, implying the same crosslinking observed in the case of ParG-K11C (Figures 24a, 25a and 26a).

The visible bands are all much weaker than was observed in ParG-K11C reactions of the same type, suggesting that the formation of higher order structures was reduced.

56

Unfortunately, this is not possible to clearly identify the cause as the entire lane above 35 kDa is heavily smeared and difficult to distinguish. I attribute this to the contaminant proteins visualised in the bands in the ParG-K12C aliquot. Any contaminant that contains cysteine would be capable of crosslinking to the ParG-K12C cysteines resulting in the smear due to unknown proteins in an array of possible combinations.

The ParF-K155C protein samples showed a presence of 14 kDa contaminant band similar to that of the K11C-K160C crosslinking gels (Figures 25 and 26). Though these gels also showed a faint band of protein at the correct molecular mass of ParF. This ParF-K155C band is encouraging as it would be expected with a successful dialysis and demonstrates that the ParF proteins can be successfully dialysed. This corroborates the hypothesis that the loss occurred after the dialysis.
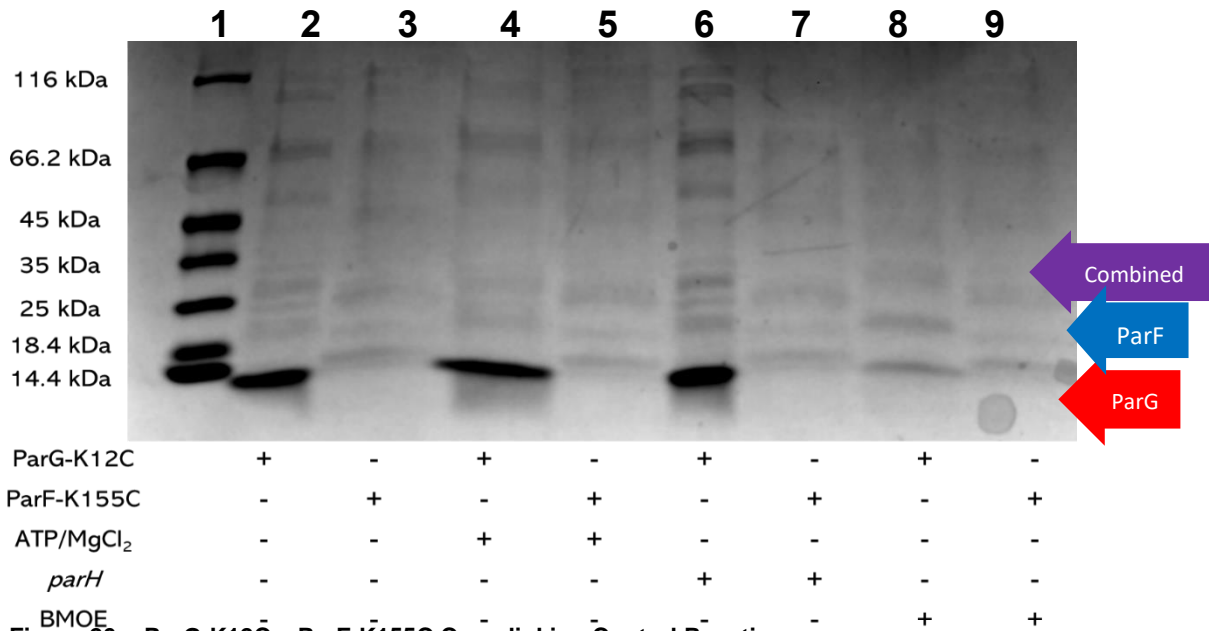
Figure 26a: ParG-K12C – ParF-K155C Crosslinking Control Reactions

	1	2	3	4	5	6	7	8	9
ParG-K12C		+	-	+	-	+	-	+	-
ParF-K155C		-	+	-	+	-	+	-	+
ATP/MgCl$_2$		-	-	+	+	-	-	-	-
parH		-	-	-	-	+	+	-	-
BMOE		-	-	-	-	-	-	+	+

4-15% SDS-PAGE gel showing protein profile of control crosslinking reactions consisting of one of ParG-K12C or ParF-K155C in conjunction with cofactor molecules and BMOE crosslinker as detailed in section 2.2.2.

Legend: + indicates the presence of the protein, cofactor or crosslinker in the reaction. – indicates it is absent in the reaction, the arrows show the expected mass of both proteins' monomers and of their combined mass.
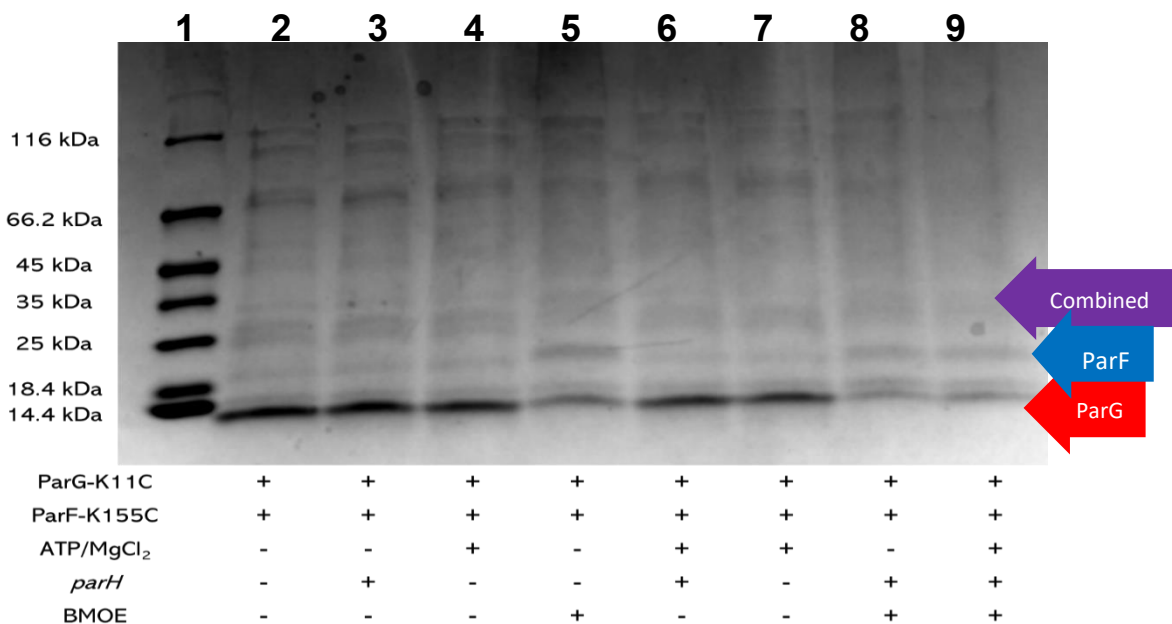
Figure 26b: ParG-K12C – ParF-K155C Crosslinking Treatment Reactions

	1	2	3	4	5	6	7	8	9
ParG-K11C		+	+	+	+	+	+	+	+
ParF-K155C		+	+	+	+	+	+	+	+
ATP/MgCl$_2$		-	-	+	-	+	+	-	+
parH		-	+	-	-	+	-	+	+
BMOE		-	-	-	+	-	-	+	+

4-15% SDS-PAGE gel showing protein profile of treatment crosslinking reactions consisting of both ParG-K12C and ParF-K155C in conjunction with cofactor molecules and BMOE crosslinker as detailed in section 2.2.2. **Legend**: + indicates the presence of the protein, cofactor or crosslinker in the reaction. – indicates it is absent in the reaction, the arrows show the expected mass of both proteins' monomers and of their combined mass

None of the cofactor molecules had any visible effect on the ParF-K155C band. There was also very little change in the band intensity of the ParF-K155C band when exposed to BMOE. Although the lanes 8 and 9 demonstrated a smear that passed heavier than 116 kDa, this only shows that crosslinking was successfully occurring in the contaminants of the reactions. The aforementioned significant contaminant band did not change strength, showing a lack of interaction due to the presence of BMOE.

The treatment gel showed faint but much more distinct ParF-K155C bands than previous gels. They did not show any clear interaction with cofactor molecules, though it is unclear whether this is due to a genuine lack of interaction or that the bands are too weak for visible changes (Figure 26b).

The gel in figures 26a and 26b show bands of around 15 kDa that were visibly distinct from the ParG-K12C bands in all lanes with a ParF fraction present. This band is an unknown contaminant protein, though due to its intensity not being visibly affected by the addition of BMOE, it is unlikely to be interfering with the crosslinking and therefore is unlikely to feature a cytosine residue. This would eliminate the chicken egg white lysozyme as the protein in question (64). Due to this lack of data, the identity of the contaminant cannot be determined. Even if contaminating crosslinking were occurring, there is no visible evidence on this gel and the results are already marred by the presence of the ladder resulting from the chain crosslinking as described in figure 24.

The gels present a ParG homodimer band in lane 8 of the control gel and lanes 5, 8 and 9 of the treatment gel, showing that crosslinking was not affected by any protein in the ParF-K155C sample. There was visible crosslinking of a 20 kDa contaminant protein as the band was absent in the above lanes but presented slightly below 30 kDa, its visibility suggesting heteromeric crosslinking with the ParG-K11C.

The band generated by the ParG-K12C dimer mass crosslinking product was less intense in the reactions that contained *parH*. This provides evidence that ParG-K12C formed higher order structures when *parH* was present. Although the high amount of contaminant protein makes it impossible to determine this for certain, it merits further investigation in future work.

These gels showed a loss of ParF consistent with previous gels and had a high amount of visible contaminant in the ParG-K12C samples, this made well defined conclusions difficult to assert.

3.3.5 ParG-K12C – ParF-K160C

The crosslinking data in ParG-K12C and ParF-K160C reactions were difficult to obtain due to poor quality of gels. One of these gels shows a distinction in the ParF-K160C sample that was not visible in a later, more successful gel due to lower gel quality (Figures 27 and 28b).

This gel generated a bleaching effect that completely obscured any protein above 16 kDa, making it impossible to draw conclusions about crosslinking behaviour or the presence of ParF-K160C or contaminant proteins. This gel does show the presence of the unknown contaminant in the ParF-K160C sample, which is unclear in later gels. It also shows the presence of ParG-K12C. Due to the equal amount of bleaching in every lane of Figure 27, this was concluded to be a technical error in the gel running and not due to the reactants. Despite not being effective in portraying an accurate profile of these reactions, this gel does demonstrate the presence of the two distinct bands of low molecular weight in the reactions that were performed.
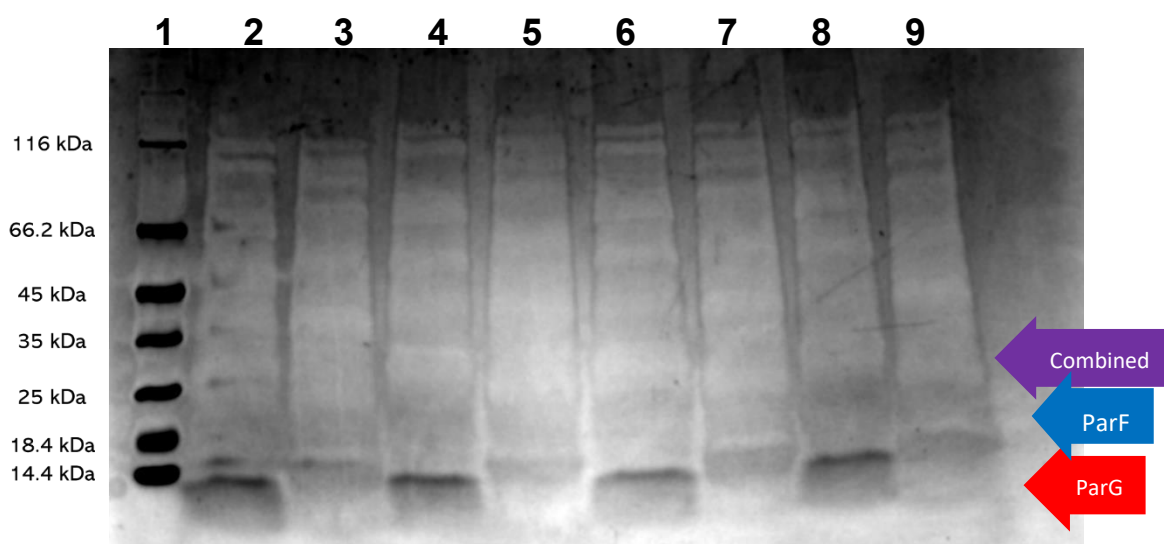
	2	3	4	5	6	7	8	9
ParG-K12C	+	-	+	-	+	-	+	-
ParF-K160C	-	+	-	+	-	+	-	+
ATP/MgCl$_2$	-	-	+	+	-	-	-	-
parH	-	-	-	-	+	+	-	-
BMOE	-	-	-	-	-	-	+	+

Figure 27: ParG-K12C – ParF-K160C Bleached Crosslinking Control Reactions

4-15% SDS-PAGE gel showing bleached protein profile of control crosslinking reactions consisting of one of ParG-K12C or ParF-K160C in conjunction with cofactor molecules and BMOE crosslinker as detailed in section 2.2.2. **Legend**: + indicates the presence of the protein, cofactor or crosslinker in the reaction. – indicates it is absent in the reaction, the arrows show the expected mass of both proteins' monomers and of their combined mass.

Due to the highest concentration sample of ParF-K160C being depleted, the ParF-K160C used in the reactions shown in these gel images was taken from two different samples. The

later reactions in Figure 28b use the same sample as was seen in Figure 25 and showed no visible ParF protein. The sample used in the reactions of Figure 28a and the first two reactions of Figure 28b did show a strong presence of ParF protein. Both of these samples had been purified, dialysed and stored identically and both were made up to the same concentration for the reaction. Although this shows that the ParF-K160C can be retained following freezing and storage, it is unclear why this sample was not lost. This does allow for more informative gels to be undertake in future studies.

The results on the unbleached control gels are less clear than previous reaction experiments. The gel appears to have bent downwards, giving a skewed approximation of the band weights and losing a portion of the ParG-K12C protein in lanes 6 and 8 of Figure 28a. This obscured any data that can be determined from them regarding ParG-K12C (Figure 28a).

Lane 9 of the control reaction gel showed a significant reduction in the thickness of the ParF-K160C monomer band compared to lanes 3 and 7. It also showed a faint protein presence slightly below 45 kDa at the molecular mass that would match that of the ParF-K160C homodimer that was absent in other ParF-K160C bands in this gel, suggesting homomeric crosslinking. A similar but less pronounced decrease in lane 5 corroborates this, as both could feasibly be showing dimerisation via different mechanisms. This gel also shows a lack of unknown band in the new sample of ParF-K160C despite the concentration being the same as all previous gels that showed a presence of it (Figures 26, 25, 27 and 28)

The apparent absence of the contaminant band in the treatment gel is only certain lanes 2 and 3 of the treatment gel. Comparison to the control gels in the bleached gels is more appropriate in the later reactions. The bleached gel confirms the assertions from Figure 25 that the ParF-K160C sample contains the contaminant which further obscures the role of ParG-K12C in these reactions.

The treatment gel lane quality is very poor and there are no distinct visible bands other than the ParF monomers in lanes 2 and 3. There are no reactions in this gel that include BMOE and have a visible ParF protein presence or a ParG ban that is not contaminated. There is a visible reduction in the ParG monomer band in lane 8. This could be presenting crosslinking but without any other visible bands no further conclusions can be drawn based on the data in this gel.
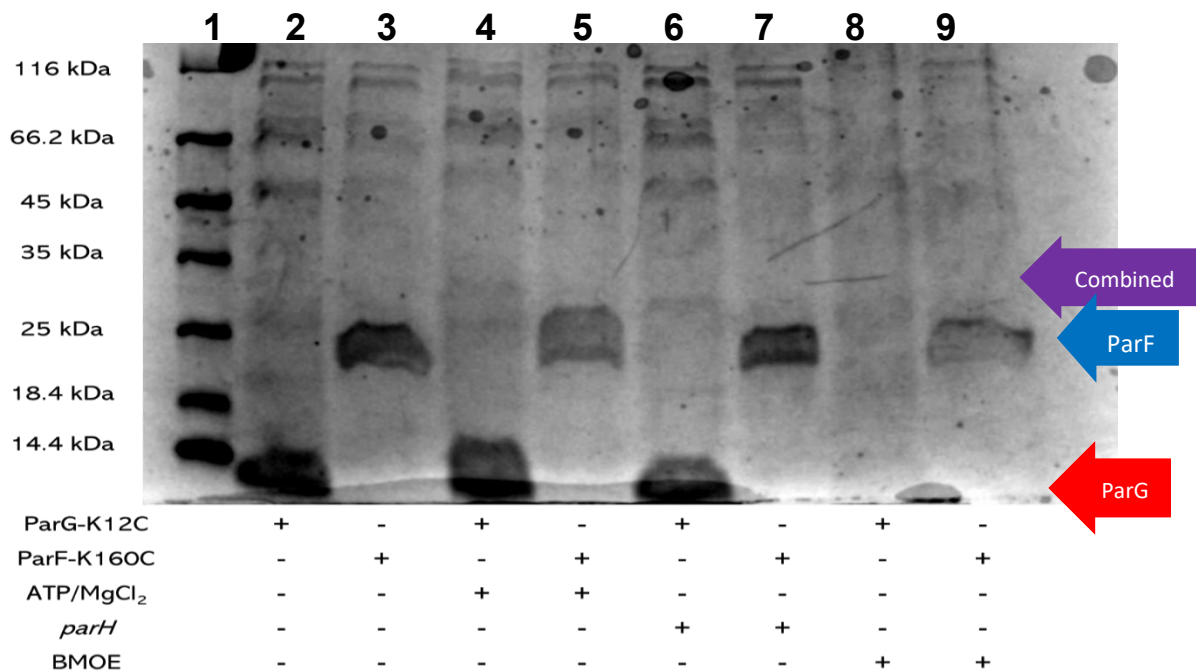
Figure 28a: ParG-K12C – ParF-K160C Crosslinking Control Reactions

4-15% SDS-PAGE gel showing protein profile of control crosslinking reactions consisting of one of ParG-K12C or ParF-K160C in conjunction with cofactor molecules and BMOE crosslinker as detailed in section 2.2.2.

Legend: + indicates the presence of the protein, cofactor or crosslinker in the reaction. – indicates it is absent in the reaction, the arrows show the expected mass of both proteins' monomers and of their combined mass.
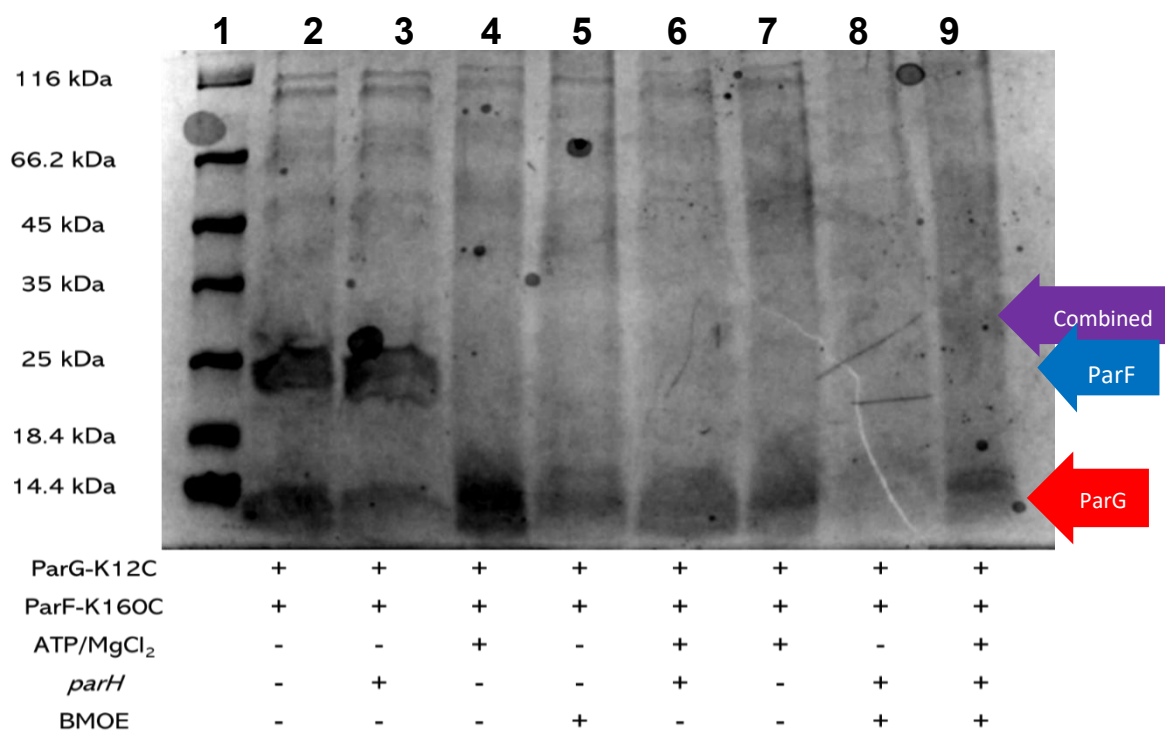
Figure 28b: ParG-K12C – ParF-K16OC Crosslinking Treatment Reactions

4-15% SDS-PAGE gel showing protein profile of treatment crosslinking reactions consisting of both ParG-K12C and ParF-K16OC in conjunction with cofactor molecules and BMOE crosslinker as detailed in section 2.2.2. **Legend**: + indicates the presence of the protein, cofactor or crosslinker in the reaction. – indicates it is absent in the reaction, the arrows show the expected mass of both proteins' monomers and of their combined mass

Chapter 4:

Conclusion and Future Work

There were several challenges across this project that prevented useful determination of the desired data. Despite this, there was also a useful amount of data gained from it on how to pursue this question more adequately in the future.

The mutagenesis of the plasmids was broadly successful, the only difficulties occurred in attempting to generate the plasmids in high enough concentrations to sequence them. Several attempts at preparing purified plasmids were sufficient for all plasmids aside from the *parG-K12C* plasmid which required pooling of multiple plasmid purifications and concentrating them. This was very effective and generated a high concentration of plasmids that were sequenced and subsequently expressed in transformant cells. Transformation of the plasmids also occurred with very little difficulty, with no instances of failed transformations. Though there were several occurrences of overproduction data being inconclusive, there were no outright failures and every transformed sample grew successfully in the presence of ampicillin. The only issue in protein production was a minor issue in which a single sample of ParG-K12C appeared to be insoluble. This was overcome with a repeat that used a less intensive sonication protocol.

There were several significant oversights in this study both in design and execution. Initially, it would have been prudent to measure the ratio of absorbance of the DNA at 260 and 280 nm to ensure that the DNA is not at fault for the quality of protein that presented the major issues in this study. This could not be performed as DNA was not available in high enough purity or amount to both perform such analyses and transform into the cells. There were several missed opportunities with regard to control experiments that should have been included, most notably a lack of repeats of gels that demonstrated meaningful results or re-runs of gels that were of low running quality or low image quality, though this was primarily due to the continued failure of protein storage, it should have been prioritised to improve the reliability and reproducibility of this study. This demonstrates the need for refining the protocol further to obtain and then maintain higher amounts of the target proteins.

Protein purification demonstrated several failures. Initially, mutant proteins were lost due to high concentration of imidazole in the buffers and obscured in gel images due to dilution in the 50 mL volumes of binding and wash buffer which required adjustment of the buffers to overcome, as mentioned in section 2.1.2. The issue of DTT in the storage buffer also had to be addressed but could not be done chemically so samples were discarded and purifications were reattempted using the new protocol with an adjusted storage buffer, also mentioned in section 2.1.2.

The most significant issue was that the majority of the ParF proteins were not visible in the gel images following the crosslinking experiments. Though initial post-purification gels showed strong ParF presences, subsequent samples of ParF, wild-type and mutant, showed a loss of visible protein on gel images. This shows that the method is lacking in catering to the molecular needs of the protein following purification. Figures 22a and 22b in particular show a decrease in visibility of these proteins; though 22b shows some more visible bands in lanes 8 and 9. Subsequent gels 25a, 26a and 28a all demonstrate a much clearer visible presence of the protein across the gels, most notably in their respective third lanes, where no other chemical was added, clearly demonstrating the presence of the proteins in the gels. The lack of visible ParF proteins in the crosslinking gels precluded any adequate conclusions regarding the interaction of the two proteins.

Though some reduction in concentration would normally expected in a dialysis, the adjusted proportion of glycerol made to the storage buffer for the ParG-K11C and ParG-K12C noted in section 3.2.5 and 3.2.6 should have assuaged any concentration issue with ParF when it was mixed. I have concluded that the most likely candidate for the step that caused the loss of the various ParF proteins was the freezing and storage process. This could be related to the stability of the ParF being more severely impacted post-purification than other visible proteins and may have resulted in aggregation as a result of cold sensitivity. If the error were due to an error in the dialysis, it would have affected more proteins, including the ParG and any contaminants. The protein loss is also unlikely to be due to any proteases due to the lack of native *lon* and *ompT* genes for proteases encoded by the BL21(DE3) cell line (55). It is also unlikely to be due to sonication-induced aggregation reducing the visibility on the gels as this issue occurred and was corrected, as discussed above.

In considerations for further studies, it is likely that correcting the issue of stable ParF storage will require performing dialyses and crosslinking reactions immediately following purification on combined purification fractions where ParF is known to elute best. This would prevent the need for freezing or prolonged periods of storage in cold environments that could contribute to protein loss if a similar study is attempted on these proteins in future.

Another possible recommendation for attempting to increase the stability of ParF in future studies would be an overhaul of the storage mechanisms or to determine if the ParF has a higher cold sensitivity than ParG and is aggregating following thawing. This could be tested through comparison of multiple aliquots of protein from the same purification that would be freeze-thawed a varying number of times. In the case that freezing is causing aggregation, treatment with a non-denaturing detergent such as Tween 20 or CHAPS following purification, rather than freezing the samples, could be used to attempt to maintain the

proteins' solubility and could be compared to the result of this study to attempt to detect any cold sensitivity or freeze-thaw leading to aggregation. If this proves a significant difference, it would become prudent to perform a Bradford assay and crosslink the ParF immediately following dialysis so as to omit the need for the detergent treatment or freezing and storage steps altogether. This method also presents a possible alternative to the aforementioned issue of being unable to measure sample purity and concentration following freeze-thaws by omitting the freeze-thaws entirely.

Unfortunately, without more information, it is not possible to identify the specific factor that prevented the protein from surviving the process but these recommendations would potentially clarify the reasons that ParF failed to purify reliably throughout this study and present an adequate solution to prevent it in future.

Despite no conclusive evidence that would elucidate the effect of the cofactors on the interaction, testing this reaction in further studies should use an alternative non-hydrolysable ATP alternative such as AppNHp or AppCp as an additional control. This would better showcase the difference in interaction as ParG mutants could trigger the ParF ATPase activity and have no ParF in its ATP bound conformation when the BMOE is added. This could better elucidate any role the conformation of ParF plays in its interaction with ParG. An ATP control should also be used to show any effect of conformation on interaction.

There was another significant design failure in failing to adequately consider the impact of the native cysteine at position 53 in the WT ParG protein during the developmental phases of the study. This was an oversight that had a fundamental impact on the results collected. The residue had significant impacts on the crosslinking behaviour of the collected samples, resulting in homomeric crosslinking observed in all variants of ParG protein. The homomeric crosslinking, shown in Figures 22a, 23a and 26a, demonstrate that both the native C53 and mutant cysteines on the N-terminal tail are capable of crosslinking. Particularly in the ParG-K11C and ParG-K12C that demonstrated a chained crosslinking of more than a dimer in lane 8 of Figures 23a and 25a, expressed by a proposed mechanism as modelled in Figure 24. Unfortunately, this also makes specifics on observed heteromeric interaction with ParF mutants less reliable as it is impossible to distinguish which cysteine residue would be interacting with the ParF site. It would be necessary to control for behaviours of these proteins in future studies, one such method would be to mutate C53 to a residue that does not contain sulphur, I would suggest serine be used as it shares the charge and shape of cysteine but would not be amenable to BMOE crosslinking. This method would initially require its own control experiments to determine efficacy. If a C53S mutant is not successful then including a control reaction of WT ParG with any ParF mutants could be used as an

alternate control. This would allow comparison of the rates of crosslinking to determine how much of the ParF mutant was binding to each ParG cysteine. Though it is worth noting that this behaviour does clarify that crosslinking is a valid method of observing the interaction of such proteins and that, given alterations to the experimental procedure, it could be an effective method to use to determine the residues most vital to the interaction of these two proteins and the *parH* region in further study.

Another significant issue of this study is that of the sample protein purity. Low visibility of sample proteins and presence of contaminants in the images throughout this study prevented accurate determinations of the behaviours of the proteins and contributed to the low gel quality and lack of repeated gel runs throughout the results that was caused by low availability of target proteins.

An example of the issue of purity would be of the aforementioned contaminant band that appeared in ParF-K160C samples. It is faintly visible in the crosslinking gels but is not visible in the purification gels. Experimental repeats could allow for distinct characterisation of this band or to demonstrate that it is not present, such as in gels that display batch behaviour that differs to comparable data or additional bands, such as in Figure 25b. If this band is found to be lysozyme acting as a contaminant, it could be omitted in favour of a non-contaminating mechanical process, I would suggest a lower intensity sonication for more cycles of sonication to prevent aggregation or damage to the proteins. As noted earlier, lower intensity sonication reduced the rate of aggregation in ParG-K12C and it would be inadvisable to increase intensity for this reason. It would also eliminate the aforementioned hypothesised cause of the significant contaminant in the ParF-K160C sample being ParF protein that was damaged by sonication. Improving the purity of the samples would require alterations to the purification protocols. In future studies, this could be achieved by increasing the amount of resin and binding buffer used in TAP purification as it would result in a greater amount of bound protein, this would require a longer cycling time during the binding phase to maximise efficacy of the increased gel. To optimise the elution step, a higher concentration of glycerol in the storage buffer would increase concentration of any protein recovered, similarly to its use in the purifications of the ParG mutant proteins (61). If sample purity and volume can be substantially improved, it would allow for more repeats of experiments including concentration analyses and crosslinking experiments as well as improving both the quality and reproducibility of gel images. Additionally, it would allow for a greater array of tests such as quality testing of the DNA to provide additional data that could elucidate issues in the study. A greater amount of reliable data would allow for more accurate characterisation of the proteins under inspection, both sample and contaminant,

which would allow for more robust conclusions and give a clearer characterisation of the interaction site of ParF and ParG.

With regard to the aims of the study, probing the interaction site of ParF and ParG, this study has not been successful. A lack of clear gel images and insufficient time to correct issues in the protocols to generate such images meant that the results in the gels were not sufficient to draw any concrete conclusions regarding the ParFG*H* system itself. The only occurrence of heteromeric crosslinking in the study was a single band in the ParG-K12C – ParF-K155C gels in lane 5 of Figure 26b. This cannot be used to reliably draw any conclusions about the interaction of the proteins due to a lack of control and no repeats.

What has been gained from this study is clarification on the efficacy of some of the protocols. BMOE proved successful in creating crosslinks between cysteine residues on different proteins, albeit primarily homomeric crosslinking of ParG. It also demonstrated successful mutagenesis and overproduction of the proteins and determined some initial refinements for potentially overcoming the shortcomings of this study regarding purification. The lack of repeats and low quality of gels was a significant issue in this project due to timing constraints preventing repeats from being attempted. In future studies on this interaction, it would be imperative to obtain more repeats of results, to improve the validity of any conclusions.

This study has clarified several key flaws in the experimental process that must be corrected in order to adequately perform research in this system moving forwards. With regard to the impact of information determined by this study on the broader field of the partitioning system, there is not enough to assist in the development of any method of affecting the ParFG*H* system. Thereby, I would advise that future research on this system utilise the initial transformation and purification methods that proved effective in this study and to use the adjustments that I have recommended in this chapter. If more specific information regarding the interaction site could be determined. Unfortunately, as I have summarised thus far, this study is lacking on providing the necessary definite data to make any such conclusions and is merely able to inform future studies towards this goal.

References

1.   Vinnichenko G, Jarrett AJM, Hope JM, Brocks JJ. (2020). Discovery of the oldest known biomarkers provides evidence for phototrophic bacteria in the 1.73 Ga Wollogorang Formation, Australia. Geobiology. 18(5): 544-559

2.   Granato ET, Meiller-Legrand TA, Foster KR. (2019). The Evolution and Ecology of Bacterial Warfare. Current Biology. 29(11): 521-537

3.   Nair RR, Vasse M, Wielgoss S, Sun L, Yu YN, Velicer GJ. (2019). Bacterial predatorprey coevolution accelerates genome evolution and selects on virulence-associated prey defences. Nature Communications. [Internet]. [Updated 9.2020; cited 11.2021]. Available from: https://doi.org/10.1038/s41467-019-12140-6

4.   Sentchilo V, Mayer AP, Guy L, Miyazaki R, Tringe SG, Barry K, Malfatti S, Goessmann A, Robinson-Rechavi M, van der Meer JR. (2013). Comminity-wide plasmid gene mobilization and selection. ISME Journal. 7: 1173-1186

5.   Eberhard WG. (1990). Evolution in Bacterial Plasmids and Levels of Selection. University of Chicago Press Journals: Quarterly Review of Biology. 65(1)

6.   Thomas CM, Nielsen KM. (2005). Mechanisms of, and Barriers to, Horizontal Gene Transfer between Bacteria. Nature Reviews: Microbiology. 3: 711-721

7.   Smalla K, Jechalke S, Top EM. (2021). Plasmid Detection, Characterization, and Ecology. Microbiology Spectrum. [Internet]. [Updated 1.2021; cited 11.2021]. Available from: https://doi.org/10.1128/microbiolspec.PLAS-0038-2014

8.   Gemski P, Lazere JR, Casey T, Wohlhieter JA. (2021). Presence of a virulenceassociated plasmid in *Yersinia pseudotuberculosis*. [Internet]. [Updated 2.2021; cited 11.2021]. Available from: https://doi.org/10.1128/iai.28.3.1044-1047.1980

9.   Lacey RW. (1975). Antibiotic Resistance Plasmids of *Staphylococcus aureus* and Their Clinical Importance. Bacteriological Reviews. 39(1): 1-32

10.   Smith M, Sockett R. (1999). Genetic Methods for Diverse Prokaryotes. Methods in Microbiology. vol. 29. Academic Press. pp. 75–77

11.   Matsunaga F, Ishiai M, Kobayashi G, Uga H, Yura T, Wada C. (1997). The central region of *RepE* initiator protein of mini-F plasmid plays a crucial role in dimerization required for negative replication control. Journal of Molecular Biology. 1(21): 27-38

12.   Wang Y, Penkul P, Milstien JN. (2016). Quantitative Localization Microscopy Reveals a Novel Organization of a High-Copy Number Plasmid. Biophysical Journal. 111(3): 467-479

13.   Paulson J, Chattoraj DK. (2002). Control of plasmid DNA replication by iterons: no longer paradoxical. Molecular Microbiology. 37(3): https://doi.org/10.1046/j.13652958.2000.01986.x

14.   Williams R, Thomas CM. (1992). Active partitioning of bacterial plasmids. Journal of General Microbiology. 136: 1-16

15.   Lehnherr H, Maguin E, Jafri S, Yarmolinsky MB. (1993). Plasmid addiction genes of bacteriophage P1: *doc*, which causes cell death on curing of prophage, and *phd*,

which prevents host death when prophage is retained. Journal of Molecular Biology. 233(3):414428

16. Sengupta M, Nielson HJ, Youngren B, Austin S. (2010). P1 Plasmid Segregation: Accurate Redistribution by Dynamic Plasmid Pairing and Separation. Journal of Bacteriology. 192(5): 1175-1183

17. Arbing MA, Handelman SK, Kuzin AP, Verdon G, Wang C, Rothenbacher FP, Abshidze M, Liu M, Hurley JM, Xiao R, Actono T, Inouye M, Montelione GT, Woychik NA, Hunt JF. (2010). Crystal Structures of Phd-Doc, HigA, and YeeU Establish Multiple Evolutionary Links between Microbial Growth-Regulating Toxin-Antitoxin Systems. Cell Press. 18(8): 996-1010

18. Dmowski M, Jagura-Burdzy G. (2013). Active stable maintenance functions in low copy-number plasmids of Gram-positive bacteria I. Partition systems. Polish Journal of Microbiology. 62(1): 3-16

19. Gordon GS, Sitnikov D, Webb CD, Teleman A, Straight A, Losick R, Murray AW, Wright A. (1997). Chromosome and low copy plasmid segregation in *E. coli*: visual evidence for distinct mechanisms. Cell. 90(6): 1113–1122

20. Summers DK. (1991). The Kinetics of Plasmid Loss. Trends in Biotechnology. 9(1): 273-278.

21. Schumacher MA. (2007). Structural biology of plasmid segregation proteins. Current Opinion in Structural Biology. 17(1): 103–110

22. Surtees JA, Funnell BE. (2003). Plasmid and Chromosome Traffic Control: How ParA and ParB Drive Partition. Current Topics in Developmental Biology. 56: 145-180

23. Aylett CHS, Izoré T, Amos LA, Löwe J. (2013). Structure of the Tubulin/FtsZ-Like Protein TubZ from Pseudomonas Bacteriophage ΦKZ. Journal of Molecular Biology. 423(12): 2164-2173.

24. Oliva, M.A., Martin-Galiano, A.J., Sakaguchi, Y., and Andreu, J.M. (2012) Tubulin homolog TubZ in a phage-encoded partition system. Proceedings of the National Academy of Sciences of the United States of America. 109(20): 7711-7716

25. Hayashi I. (2020). The C-terminal region of the plasmid partitioning protein TubY is a tetramer that can bind membranes and DNA. Journal of Biological Chemistry. 295(51): 17770-17780

26. Garner EC, Campbell CS, Mullins RD. 2004. Dynamic instability in a DNAsegregating prokaryotic actin homolog. Science. 306(5698): 1021-1025

27. Gerdes K, Larsen JE, Molin S. 1985. Stable inheritance of plasmid R1 requires two different loci. Journal of Bacteriology. 161(1): 292-298

28. Hanson PI, Whiteheart SW. 2005. AAA+ proteins: have engine, will work. Nature Reviews Molecular Cell Biology. 6: 519-529

29. Funnell BE, Gagnier L. 1993. The P1 Plasmid Partition Complex at parS: Analysis of ParB protein binding activity and specificity. Journal of Biochemistry. 268(5): 3616-3624

30.   Golovanov AP, Barillà D, Golovanova M, Hayes F, Lian LY. (2003). ParG, a protein required for active partition of bacterial plasmids, has a dimeric ribbon–helix–helix structure. Molecular Microbiology. 50(4): 1141-1154

31.   Centre for Disease Control and Prevention. Salmonella Infections Linked to Onions. [Internet]. Altanta, Georgia, Unides States of America. [Updated 10.2020; cited 12.2021]. Available from: https://www.cdc.gov/salmonella/newport-07-20/

32.   Centre for Disease Control and Prevention. Salmonella Homepage. [Internet]. Altanta, Georgia, Unides States of America. [Updated 10.2020; cited 12.2021]. Available from: https://www.cdc.gov/salmonella/index.html

33.   Barillà D, Rosenberg MF, Nobbmann U, Hayes F. (2005). Bacterial DNA segregation dynamics mediated by the polymerizing protein ParF. The EMBO Journal. 24: 1453-1465

34.   Schumacher MA, Ye Q, Barge MT, Zampini M, Barillà D, Hayes F. (2012). Structural Mechanism of ATP-induced Polymerization of the Partition Factor ParF. Journal of Biological Chemistry. 287(31): 26146-26154

35.   Lutkenhaus J, Sundaramoorthy M. (2003). MinD and role of the deviant Walker A motif, dimerization, and membrane binding in oscillation. Molecular Microbiology. 48(2): 295304

36.   Caccamo M, Dobruk-Serkowska A, Rodríguez-Castañeda F, Pennica C, Barillà D, Hayes F. (2020) Genome Segregation by the Venus Flytrap Mechanism: Probing the Interaction Between the ParF ATPase and the ParG Centromere Binding Protein. Frontiers in Molecular Biosciences. 7(108)

37.   Dobruk-Serkowska A, Caccamo M, Rodríguez-Castañeda F, Wu M, Bryce K, Ng, I, Schumacher, M. A, Barillà, D, Hayes F. (2012). Uncoupling of nucleotide hydrolysis and polymerization in the para protein superfamily disrupts DNA segregation dynamics. Journal of Biological Chemistry. 287(51): 42545-42554

38.   Jalal ASB, Le TBK. (2020). Bacterial chromosome segregation by the ParABS system. Open Biology. 10(6):200097 10.1098/rsob.200097

39.   Vecchiarelli AG, Havey JC, Ing LL, Wong EOY, Waples WG, Funnell BE. (2013). Dissection of the ATPase Active Site of P1 ParA Reveals Multiple Active Forms Essential for Plasmid Partition. Journal of Biological Chemisty. 288(24): 17823-17832

40.   Breg JN, van Opheusden JH, Burgering MJ, Boelens R, Kaptein R. (1990). Structure of Arc repressor in solution: evidence for a family of beta-sheet DNA-binding proteins. Nature. 346(6284): 586-589

41.   Augustus AM, Reardon PN, Spicer LD. (2009). MetJ repressor interactions with DNA probed by in-cell NMR. Proceedings of the National Academy of Sciences of the United States of America. 106(13): 5065-5069

42.   Carmelo E, Barillà D, Golovanov AP, Lian LY, Derome A, Hayes F. (2005). The unstructured N-terminal tail of ParG modulates assembly of a quaternary nucleoprotein complex in transcription repression. Journal of Biological Chemistry. 280(31): 28683-28691

43. Barillà D, Carmelo E, Hayes F. (2007). The tail of the ParG DNA segregation protein remodels ParF polymers and enhances ATP hydrolysis via an arginine finger-like motif. PNAS. 104(6): 1811-1816

44. Yates P, Lane D, Biek DP. (1999). The F plasmid centromere, sopC, is required for full repression of the sopAB operon. Journal of Molecular Biology 290(3): 627–639

45. Castaing JP, Bouet JY, Lane DF. (2008). Plasmid partition depends on interaction of SopA with non-specific DNA. Molecular Microbiology. 70(4): 1000–1011

46. McLeod BN, Allison-Gamble GE, Barge MT, Tonthat NK, Schumacher MA, Hayes F. (2017). A three-dimensional ParF meshwork assembles through the nucleoid to mediate plasmid segregation. Nucleic Acids Research.

47. Gerdes K, Howard M, Szardenings F. (2010). Pushing and pulling in Prokaryotic DNA segregation. Cell. 141(6):927-942

48. Vecchiarelli AG, Neuman KC, Mizuuchi K. (2014) "A propagating ATPase gradient drives transport of surface-confined cellular cargo". PNAS USA. 111(13): 4880-4886

49. Vecchiarelli AG, Hwang LC, Mizuuchi K. (2013). "Cell-free study of F plasmid partition provides evidence for cargo transport by a diffusion-ratchet mechanism". PNAS USA. 110(15): 1390-1397

50. Vecchiarelli AG, Seol Y, Neuman KC, Mizuuchi K. (2014). "A moving ParA gradient on the nucleoid directs subcellular cargo transport via a chemophoresis force". Bioarchitecture. 4(5): 154–160

51. Ringgaard S, van Zon J, Howard M, Gerdes K. (2009). "Movement and equipositioning of plasmids by ParA filament disassembly". PNAS. 106(46): 19369-19375

52. New England Biolabs. international.neb.com [Internet]. BL21 Competent E. coli. [cited; 6.2021]. Available from: https://international.neb.com/products/c2530-bl21-competente-coli#Product%20Information

53. Hansen LH, Knudsen S, Sørensen SJ. (1998). The effect of the lacY gene on the induction of IPTG inducible promoters, studied in Escherichia coli and Pseudomonas fluorescens. Current Microbiology. 36(6): 341–347

54. Hatano T, Yamaichi Y, Niki H (2007). Oscillating focus of SopA associated with filamentous structure guides partitioning of F plasmid. Molecular Microbiology 64: 1198 – 1213

55. Jeong H, Ju Kim H, Lee SJ. (2015). Complete Genome Sequence of *Escherichia coli* Strain BL21. Genome Announcements. 3(2):134-15

56. Agilent. QuikChange Primer Design. [Internet]. Santa Clara, California, US: Agilent; [updated 2020; cited 11.2021]. Available from: https://www.agilent.com/store/primerDesignProgram.jsp#

57. QIAGEN. QIAprep® Miniprep Handbook. [Internet]. Hilden, Germany: QIAGEN; [updated 2020; cited 1.2022]. Available from: https://www.google.co.uk/url?sa=t&rct=j&q=&esrc=s&source=web&cd=&cad=rja&uact=8&ved=2ahUKEwiZqMz20p31AhWSilwKHZ4dDm0QFnoECAMQAQ&url=https%3A

%2F%2Fwww.qiagen.com%2Fus%2Fresources%2Fdownload.aspx%3Fid%3D22df6
325-9579-4aa0-819c-
788f73d81a09%26lang%3Den&usg=AOvVaw04WC2OL6hHg5LVEhrFiWge

58. Garfinkel L, Altschuld RA, Garfinkel D. (1986). Magnesium in cardiac energy meatbolism. Journal of Molecular and Cellular Cardiology. 18(10): 1003-1013.

59. Zhang H, Schumacher MA. (2017). Structures of partition protein ParA with nonspecific DNA and ParB effector reveal molecular insights into principles governing Walker-box DNA segregation. Genes and Development. 31(5):481-492

60. Cleland WW (1964). Dithiothreitol, a New Protective Reagent for SH Groups. Biochemistry. 3(4):480–2.

61. Vagenende V, Yap MGS, Trout BL. (2009). Mechanisms of Protein Stabilization and Prevention of Protein Aggregation by Glycerol. Biochemistry. 48(46): 11084-11096

62. Stathopulous PB, Scholz GA, Hwang Y, Rumfeldt JAO, Lepock JR, Meiering EM. (2008). Sonication of proteins causes formation of aggregates that resemble amyloid. Protein Science. 13(11):3017-3027

63. Zampini M, Derome A, Bailey SES, Barillà D, Hayes F. (2009). Recruitment of the ParG Segregation Protein to Different Affinity DNA Sites. Journal of Bacteriology. 191(12):3832–3841.

64. ThermoFisher. ThermoFisher Scientific Unstained Protein Molecular Weight Marker Product Information Booklet. [Internet]. Waltham, Massachusetts, United States of America. [Updated 09.2017; cited 12.2022]. Available from: https://assets.fishersci.com/TFS-Assets/LSG/manuals/MAN0011769_Unstain_Protein_Molec_Wght_Mark_UG.pdf

65. UniProt. UniProtKB - Q6LEL2 (Q6LEL2_CHICK). [Internet]. European Bioinformatics Institute. [Updated 02.2021; cited 1.2022]. Available from: https://www.uniprot.org/uniprot/Q6LEL2

66. CCP4 Project. *CCP4 Program Suite for Windows*. 2021. Winn MD, Ballard CC, Cowtan KD, Dodson EJ, Emsley P, Evans PR, Keegan RM, Krissnal EB, Leslie AGW, McCoy A, McNicholas SJ, Murshudov GN, Pannu NS, Potterson EA, Powell HR, Read RJ, Vagin A, Wilson KS. (2011). Overview of the CCP4 suite and current developments. Acta Crystallographica. 67: 235-42 [doi:10.1107/S0907444910045749]